Electrothermal Controlled-Exposure Technology

by

John Mapes Maloney

B.S. Mechanical Engineering, University of Maryland, 1999
M.S. Mechanical Engineering, University of Maryland, 2001

Submitted to the Department of Materials Science and Engineering
in partial fulfillment of the requirements for the degree of

Master of Engineering in Materials Science and Engineering

at the

MASSACHUSETTS INSTITUTE OF TECHNOLOGY

September 2006

Author .....
Department of Materials Science and Engineering
August 18, 2006

Certified by .....
Krystyn J. Van Vliet
Thomas Lord Assistant Professor of Materials Science and Engineering
Thesis Supervisor

Accepted by .....
Samuel M. Allen
POSCO Professor of Physical Metallurgy
Chair, Departmental Committee on Graduate Students

Electrothermal Controlled-Exposure Technology
by
John Mapes Maloney

Submitted to the Department of Materials Science and Engineering
on August 18, 2006, in partial fulfillment of the
requirements for the degree of
Master of Engineering in Materials Science and Engineering

Abstract

A technology is presented for exposing the contents of microfabricated cavities in a substrate. These contents are hermetically sealed until exposure is triggered by an electronic signal. The exposure mechanism uses electrothermal heating to rupture a metal membrane at one end of the cavity. The device's capability for storing a variety of contents and exposing them on demand makes it well suited for periodic exposure of new sensors as old ones degrade.

Two commercialization possibilities are investigated: biowarfare agent detection and *in vivo* glucose sensing. Both applications employ sensing mechanisms that can be miniaturized and packaged in an array. These sensors are susceptible to fouling or degradation over time from environmental factors. The controlled-exposure technology addresses this problem by periodically exposing fresh sensors. The two applications are thought to be especially favorable markets because of the need for reliable, continuous sensing.

The engineering aspects of the technology are investigated by identifying key material properties for each component of the device. The key properties for the substrate material are suggested to be its vapor permeability and suitability for cavity formation. The most important properties of the membrane are its electrical requirements (the current and voltage required to expose or "activate" the device), its strength and hermeticity, and its stability in the intended working environment. Design and materials selection approaches for optimizing these properties are presented.

Thesis Supervisor: Krystyn J. Van Vliet
Title: Thomas Lord Assistant Professor of Materials Science and Engineering

Acknowledgments

I am grateful to my advisor, Professor Krystyn Van Vliet, for her encouragement and guidance.

I am also grateful to my parents and my MEng colleagues in the Department of Materials Science and Engineering. I sincerely appreciate your support.

It is a great pleasure to recognize the hard work of the employees, past and present, of MicroCHIPS, Inc. Their insights are featured throughout this thesis.

Finally, I am indebted to Professor Michael Cima (MIT), Professor Don DeVoe (University of Maryland), Dr. John Santini (MicroCHIPS), and Dr. Norman Sheppard (MicroCHIPS) for their support of my graduate career.

Contents

List of Figures

List of Tables

Chapter 1

Introduction

Consider a “smart package”—an automated container that opens itself. It stores its contents indefinitely in a hermetically sealed environment (Figure 1-1). It has no moving parts, no mechanical components that might leak or clog. It is opened with a voltage pulse, which resistively heats and ruptures a metal membrane at one end of the container (Figure 1-2).

Multiple containers can be constructed in a batch process, and thousands could be fabricated simultaneously on a single substrate. They can be made from biocompatible and biostable materials for use in an implantable medical device. In fact, they could be constructed from many possible materials depending on the constraints of the particular application. They might be filled with any combination of circuits, sensors, macromolecules, and cells. The containers might be opened one by one, or all at once, or in any combination. Opened apertures allow the inward and outward flux of particles, fluids, light, sound, and information.

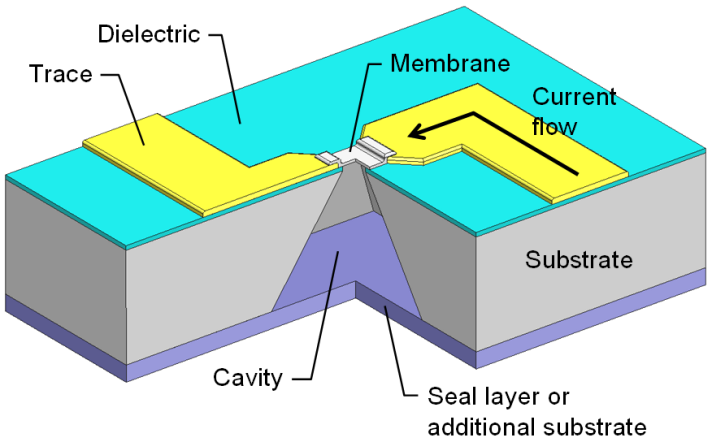

Figure 1-1: Schematic of a controlled-exposure device [1].

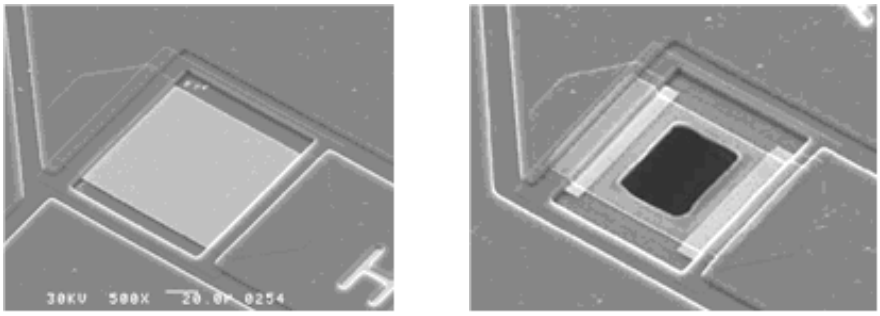

(a) (b)

Figure 1-2: Representative micrographs of 50 μm × 50 μm metal membranes (a) as fabricated and (b) after electrothermal rupture [1].

1.1 Background

This hermetic controlled-exposure concept originated in the early 1990s, when Langer and Cima conceived of a silicon microchip that could deliver drugs automatically *in vivo* [2]. Langer has recounted the origins and early development of the concept [3]:

> "About 12 years ago, I was watching a television show on PBS about how the computer industry made chips, and I started thinking that chips might be a good way to carry out drug delivery. I called Michael J. Cima, who is one of my colleagues and a professor of materials science and engineering at MIT, and asked for his help in developing a way to test the idea. We solicited the help of a student, John Santini, who began developing a drug delivery chip first as a summer project and later for his PhD thesis. Santini was able to create a chip prototype with tiny wells into which drugs could be placed. These chips offered myriad delivery possibilities. The wells might contain different doses of the same drug, or a variety of different drugs—literally, a pharmacy on a chip."

Santini's microchips, shown in Figure 1-3, contained arrays of pyramidal cavities, or reservoirs, etched in silicon. The cavities were capped with gold membranes that could be electrochemically dissolved in saline with an applied voltage [4]. At approximately +1 V relative to a saturated calomel reference electrode, the formation of soluble gold compounds in saline becomes thermodynamically favorable. The membranes thus dissolve atom by atom. Santini used this mechanism to demonstrate the storage and controlled, multiplexed release of fluorescent and radio-labeled compounds [5].

Santini considered the practical details of commercialization from the beginning, identifying key characteristics of the device such as its capability to store and release solids, liquids, and gels [4]. An operational space was outlined that considered both the dosage frequency and volume. The release of steroids or hormones for drug delivery and enzymes for immunoassays was seen to be particularly favorable because of these compounds' high activity. In 1999, Santini formed MicroCHIPS, Inc. (Bedford, MA) with Cima and Langer to commercialize this electrochemical mechanism for drug

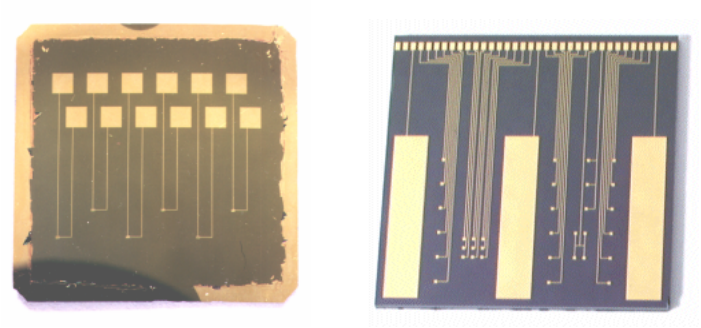

(a) (b)

Figure 1-3: Prototype microchips configured for the electrochemical mechanism [4]. Photographs by (a) Richard Holman and (b) Paul Horwitz (Atlantic Photo).

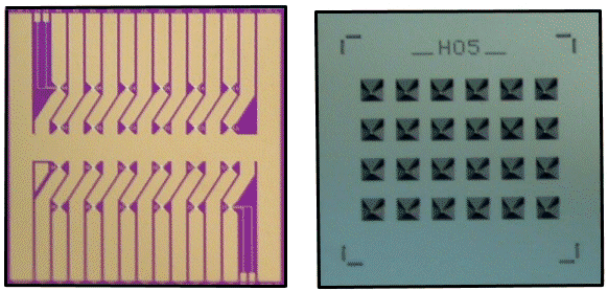

Figure 1-4: $1\,\text{cm} \times 1\,\text{cm}$, 24-cavity microchip (front and back) configured for the electrothermal mechanism [11].

delivery applications. Cima's and Langer's groups at MIT have continued to develop and demonstrate similar devices [6–8].

An alternate controlled-exposure mechanism was later invented at MicroCHIPS by Uhland and Polito [9]. This mechanism employs an electrothermal process: resistive heating from an applied current ruptures the membrane in a process similar to blowing a fuse. Operation is complete within tens of microseconds, and the typical activation current—that is, the current required to rupture the membrane and expose the cavity—is several amps. The electrothermal mechanism soon supplanted the electrochemical mechanism at MicroCHIPS for several reasons. First, the electrothermal mechanism, which is relatively energetic, is more reliable than electrochemical dissolution [10]. Second, the mechanism is independent of the surrounding medium. Third, the mechanism is faster, operating in microseconds rather than minutes [1, 6].[1]

An obvious concern about the electrothermal mechanism involves the amount of heat dissipated near the membrane and the possibility of degrading the cavity contents: the membrane is heated to its melting point during operation, and the melting temperatures of gold and titanium are above 1000°C. The thermal impact to

[1]However, the electrothermal mechanism requires orders of magnitude more current than the electrochemical mechanism and requires the device circuitry to be redesigned. The selection of materials to reduce operating current is addressed in Chapter 3.

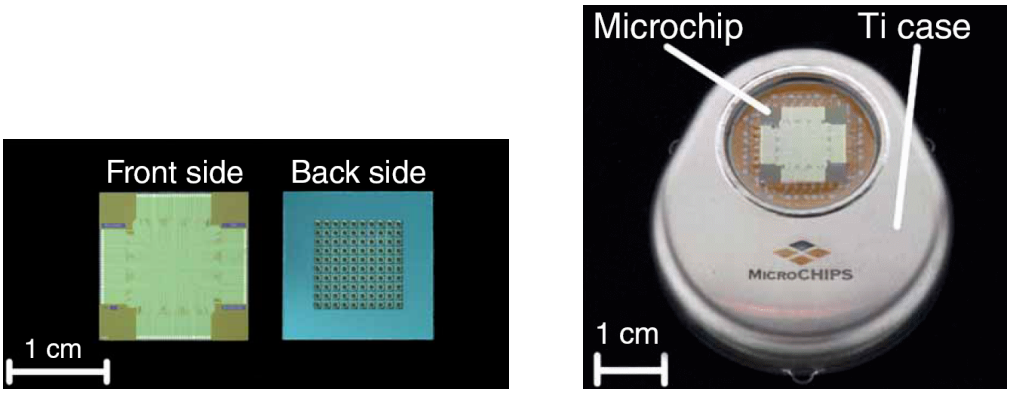

(a) (b)

Figure 1-5: (a) Representative 100-reservoir drug delivery microchips configured for the electrothermal mechanism; (b) Fully implantable drug delivery device used to demonstrate peptide release over six months in an animal model [12].

the cavity contents is limited, however, because of the brief duration of activation. The energy dissipated in the membrane area during activation can be as low as tens of microjoules, which is barely enough to heat one microgram (one nanoliter) of water by a temperature increase of 10°C. This temperature increase is usually negligible, especially because the duration of heating is brief. For the applications described in this thesis, one microgram is a negligible amount of material even for contents that could be degraded by a temperature increase of 10°C.[2]

The electrothermal mechanism has been demonstrated *in vitro* and *in vivo*. A 24-cavity microchip, shown in Figure 1-4, was packaged within a flow cell and used to release periodic doses of a radio-labeled compound *in vitro* with a coefficient of variation of 4% [1]. The mechanism was further demonstrated in a six-month *in vivo* study in which 100 to 250 μg of leuprolide was delivered weekly in beagle dogs [12]. The peptide leuprolide was chosen as a model drug; it is used in cancer treatments and has low bioavailability when given orally. The fully implantable systems used in this drug delivery study each contained a 100-cavity microchip, a microprocessor, a battery, and wireless telemetry (Figure 1-5).

As of 2006, MicroCHIPS is continuing on the path to commercialization of the electrothermal technology. The company is financed through venture capital funding and corporate partnerships, and currently has nineteen employees. Over twenty-five U.S. and non-U.S. patents have issued, and over fifty patent applications are pending [13].

[2]It is assumed here that the specific heat and density of these contents can be modeled with the properties of liquid water. Otherwise, the upper bound of the amount of material heated to a temperature difference ΔT is calculated as $E_M/cp\Delta T$, where E_M is the energy dissipated near the membrane, c is the material's specific heat, and p is the material's density.

1.2 Thesis organization

This thesis examines a technology for controlled exposure. Commercialization of drug and fragrance delivery by the electrochemical mechanism was the focus of a previous thesis [14], and is not discussed further here. Rather, the focus is on the electrothermal mechanism, which might be applied to applications other than implantable drug delivery. The thought process for conceiving alternative applications and its conclusions are described here, and several favorable applications are examined.

This thesis addresses engineering and commercialization aspects of the electrothermal mechanism. The goals are to review how the technology has been made and used, to guide the development of new devices through engineering analysis of material properties, and to outline favorable commercial opportunities. To that end, the contents are arranged as follows:

§ Device fabrication and operation are addressed in Chapter 2. Two fabrication processes are outlined for constructing silicon microchips with cavities created by wet and dry etching processes. Operation is described by presenting experimental results from MicroCHIPS' prototype devices with gold membranes.

§ A materials selection process is described in Chapter 3. The most important parameters related to the substrate and membrane are described. Modeling, experimental results, and literature reports are used to develop guidelines for optimizing performance.

§ The search for suitable applications and its results are described in Chapter 4. The capabilities and limitations of the device are summarized and the area of sensor exposure is chosen for investigation. Two favorable sensing applications, biowarfare agent detection and *in vivo* glucose sensing, are described with an overview of each field, an explanation of the technology's benefits, and a concept of technology integration.

§ Conclusions drawn from this work are summarized in Chapter 5.

Chapter 2

Device fabrication and operation

The current state of the electrothermal mechanism is reviewed in this chapter. This material is intended as a foundation for later chapters on materials selection and commercialization. Two fabrication processes are presented, and device operation is described by reviewing experimental results.

2.1 Fabrication

Briefly, controlled-exposure microchips are fabricated by depositing or growing a dielectric layer on a silicon substrate, depositing and patterning metal circuitry and membranes on one side, creating cavities by chemical etching from the back side, and removing the dielectric layer from underneath the membranes. The cavities are subsequently filled with contents for future exposure and then sealed. Santini and Johnson have described in detail the use of MIT's Microsystems Technology Laboratories for fabricating microchips configured for the electrochemical mechanism [4, 10]. Many of their processes are similar to the ones described below.

It is useful first to review the major components of the microchip:

- The **substrate** contains the cavities and supports the circuitry. All of the microchips configured for the electrochemical and electrothermal mechanisms have employed single crystal silicon as a substrate, most frequently in the starting form of four-inch wafers. Some advantages of silicon are that it is sufficiently hermetic for chemical storage, it can withstand elevated-temperature processes that occur at hundreds of degrees Celsius, it is easily incorporated into wafer-based microfabrication processing lines, and it can be chemically etched with micrometer-scale accuracy by both wet and dry methods. However, the use of other substrate materials is certainly feasible. Materials selection issues concerning the substrate are discussed further in Chapter 3.

- The **dielectric layer** electrically insulates the metal circuitry from the substrate. This layer also provides a free-standing support for the membrane during processes in which the creation of the cavities precedes membrane deposition. Alternatively, the layer serves as an etch stop to protect the membrane in cases

where the membrane is deposited before the cavities are etched. An identical layer on the opposite side of the wafer is used as a mask during cavity etching, and the selected dielectric material must therefore be resistant to the particular silicon etchant used to create the cavities. Two materials have been used so far: chemical-vapor-deposited (CVD) silicon nitride, which is resistant to aqueous silicon etchants, and thermally grown silicon dioxide, which is resistant to fluoride-based plasma etching of silicon. Both materials can be deposited simultaneously on both sides on multiple wafers in a CVD or oxidation furnace.

- The **traces** electrically connect the membrane area with wire-bond pads at the edge of the chip. These features desirably have a low electrical resistance to reduce resistive losses. The resistance is minimized by using a thickness of several microns of sputtered or evaporated gold with a 10 nm titanium adhesion layer. The traces are also designed to be as wide as possible, as shown in the chip photograph in Figure 1-4.

- The **membrane** hermetically seals the cavity until exposure is triggered. In the simplest embodiment, the membrane and traces are the same material and a single metal layer comprises both. For efficiency reasons, however, it is desirable to decouple the membrane material and thickness from the trace material and thickness. It is favorable for the membrane metal to have a relatively high resistivity to generate the maximum amount of resistive heat, a low thermal conductivity to minimize heat loss to the substrate, and a low melting temperature to minimize the temperature increase required for operation. The microchips used in MicroCHIPS' six-month animal study, for example, contained 0.3 μm-thick titanium membranes with a 10 to 20 nm layer of platinum on each side and a 10 nm titanium adhesion layer. The membrane material was predominantly titanium because of its high electrical resistivity and low thermal conductivity compared to the gold used in the traces. The platinum provided an inert coating on each side of the membrane. Both titanium and platinum have higher melting temperatures than gold; however, the changes in the other material properties were sufficient to reduce the required operational current by at least a factor of two [1]. The selection of membrane materials is discussed further in Chapter 3.

All of the materials in MicroCHIPS' devices were chosen with biocompatibility in mind, and this requirement has constrained materials selection in some cases. For example, gold is not the lowest resistivity material that could be used for the traces; however, gold is preferred for medical implantation over the more conductive silver and copper. Additionally, titanium was chosen as an adhesion layer over other possibilities such as aluminum and chromium because of the widespread use of titanium in implantable devices.

Two general fabrication processes are presented here as a foundation for later discussion of materials selection and technology commercialization. The first process relies on a single wet etching step to create the cavities. Aqueous hydroxide solutions such as potassium hydroxide (KOH) preferentially etch silicon {100} and {110}

crystallographic planes over {111} planes with a selectivity of approximately 100:1. A single-crystal silicon wafer with a {100}-oriented surface allows the creation of pyramidal holes bounded by these slower-etching {111} planes. This process is included because it was used for the experimental results described later in this chapter; additionally, both literature reports to date of the electrothermal mechanism feature microchips made using this first process [1, 12]. It is relatively simple: only one etch step is involved and the etching process does not require any tools beyond a chemical hood. Additionally, more than one wafer can be etched simultaneously in solution, which is an advantage in manufacturing.

The second process employs deep reactive ion etching (DRIE), a method of etching holes with straight sidewalls in silicon. DRIE is a multiplexed process in which the wafer is exposed to two plasma chemistries that switch every few seconds. The first, a sulfur hexafluoride chemistry, isotropically etches silicon, forming silicon tetrafluoride as a volatile etch product. The second, a fluorocarbon gas (C_4F_8), dissociates in the plasma to form a polymer layer on exposed surfaces. When the etch chemistry is reinstated, ion bombardment removes the polymer layer on the bottom of the trench and the wafer surface only. The polymer remains on the sidewalls, preventing lateral etching. Through-wafer extrusions of surface mask shapes can be created by this process.

The DRIE process presented here allows an array of openings to be constructed over a single cavity. This technique exposes more area per cavity without the strength issues that arise from simply increasing the membrane size. The process is presented because it is particularly suitable for an application in which a sensor is exposed [15]. In this case payload is not a strong constraint; rather, the primary interest is to expose a large area to maximize flux and thus reduce the sensor response time.

Fabrication by wet etching

The first fabrication process is illustrated in Figure 2-1. In (a), a silicon wafer with a {100}-oriented surface is coated with a 0.2 μm layer of silicon-rich, low-stress silicon nitride (SiN_x) by low-pressure chemical vapor deposition (LPCVD) at approximately 800°C. In (b), the silicon nitride is photolithographically patterned on the back side and a cavity is created in the substrate by wet chemical etching with aqueous KOH (25 wt%, 80°C). In (c), a titanium/gold (10 nm / 2 μm) layer is deposited by physical vapor deposition and patterned to electrically connect the cavity area to wire-bond pads at the edge of the chip. In (d), a suitable membrane material is deposited and patterned over the suspended silicon nitride. The optimal material depends on the application; previous devices have employed gold, titanium, platinum, gold-silicon, and composite membranes. Finally, in (e), the silicon nitride support is etched from the back side by plasma etching, and wire bonds are added to connect the chip to external circuitry.

Fabrication by plasma etching

The second fabrication process is illustrated in Figure 2-2. DRIE is used here with a nested mask process, in which photolithography is used to define two separate mask

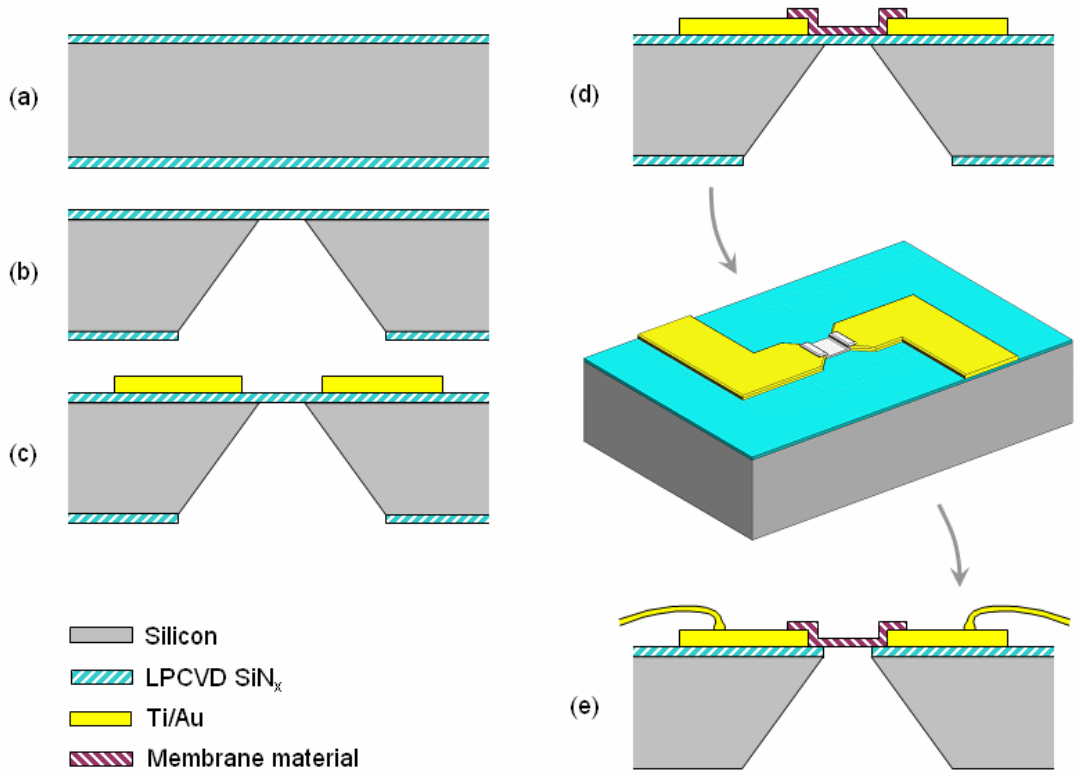

Figure 2-1: Fabrication process in which wet anisotropic etching is used to create cavities [11].

layers before etching is initiated. The first mask allows the etching of holes that will later form the suspended membrane areas. After this step, the first mask is removed, leaving the second mask defined for an additional etching step. The second etch forms the cavity. Nested masks are especially useful for processes with multiple deep etch steps, as it is difficult to spin-coat and expose photoresist uniformly on a wafer with existing cavities.

In (a), a 1 μm layer of silicon dioxide is thermally grown on a silicon wafer (the crystallographic orientation of the wafer is unimportant). Silicon dioxide is resistant to the DRIE etching chemistry with a selectivity of greater than 100:1. In (b), a titanium/gold (10 nm / 2 μm) layer and a suitable membrane material are deposited and patterned as before. In (c), the silicon dioxide layer on the back side of the wafer is patterned as a mask for the second etch. In (d), a layer of photoresist is patterned as a mask for the first etch. These two patterned layers comprise the nested mask arrangement. In (e), DRIE is used to etch holes partially through the wafer in the future suspended membrane locations. The photoresist is then removed, and a second DRIE etch is performed in (f) using the silicon dioxide as a mask. This second etch forms the cavity and removes the remaining silicon underneath the membranes. Finally, in (g), the silicon dioxide layer is etched from the back side by plasma etching, and wire bonds are attached as in the previous process.

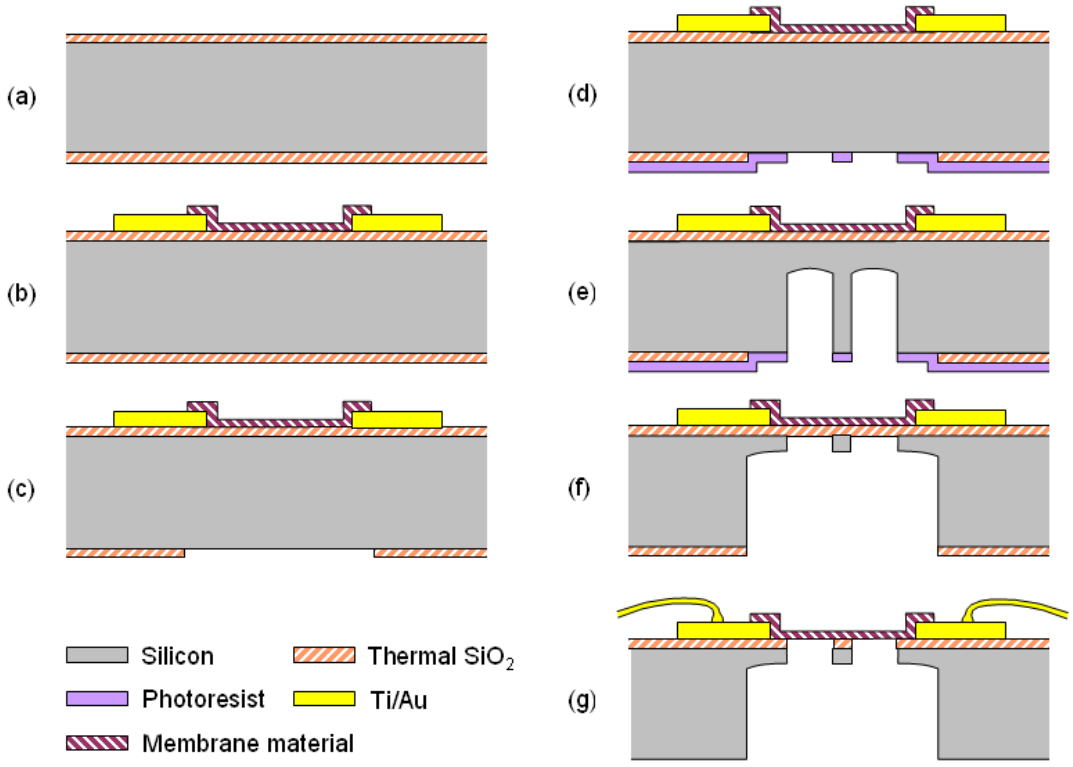

Figure 2-2: Fabrication process in which deep reactive ion etching (DRIE) is used to create cavities [11].

Incorporation of cavity contents and sealing

The cavities in the fabricated device can be filled at this point for applications in which molecules are to be released. Alternatively, an additional substrate containing sensors can be attached. The cavity can then be sealed using any one of a number of suitable low-temperature methods identified for the device [16]. In the six-month animal study performed by MicroCHIPS, the cavities were sealed by thermocompression with indium-tin solder spheres [12]. The heat dissipation during sealing was sufficiently localized and brief to not degrade the material (leuprolide) to be released. The metal-sphere-sealed configuration is illustrated in Figure 2-3, which also shows an attached borosilicate glass substrate with through-wafer holes that was added to increase the cavity volume from 120 to 300 nL.

2.2 Operation

Configuration and geometry

This section addresses the operating characteristics of the electrothermal mechanism. The microchips described here were fabricated based on the first process described earlier, in which aqueous KOH is used to etch pyramidal cavities in the substrate. The

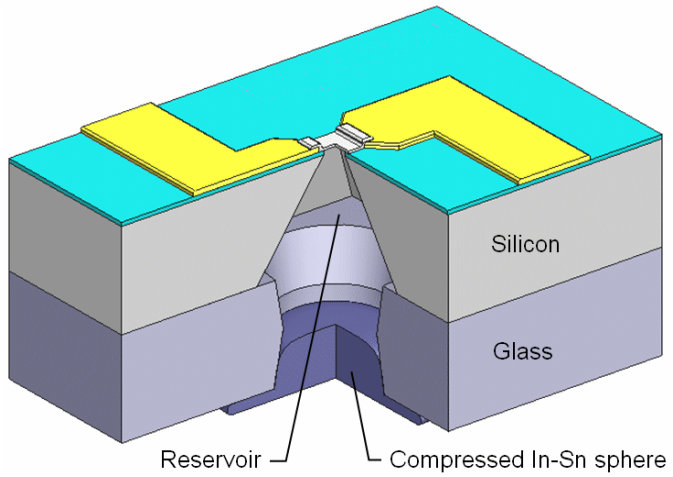

Figure 2-3: Schematic of a drug delivery reservoir sealed by an indium-tin sphere [11, 12].

process employed four-inch silicon wafers with a thickness of 525 μm. The membrane size was 50 μm × 50 μm, and the membrane material was most frequently patterned from a sputtered 0.3 μm gold layer with a titanium adhesion layer.

Membrane rupture and cavity exposure

The device operates by resistive heating as illustrated in Figure 2-4. Heating can occur preferentially in the membrane from a combination of effects. First, the membrane may be suspended in a medium such as water that is less thermally conductive than the substrate (the thermal conductivity of water ($0.6\,\mathrm{W\,m^{-1}\,K^{-1}}$) is more than two orders of magnitude smaller than that of silicon ($150\,\mathrm{W\,m^{-1}\,K^{-1}}$)). Second, the cross section of the membrane may be designed to be smaller than that of the traces to increase the local current density. A reduction in width can be seen at each membrane location in Figure 1-4. Third, the membrane may be constructed from a material with a higher electrical resistivity than that of the traces, increasing local resistive heat generation [9].

In most cases, the membrane ruptures by melting and withdrawal of molten material to the edges of the opening, where the material refreezes. This activation mode is supported by the appearance in micrographs of rounded edges forming a bead of refrozen material (Figure 1-2(b)). In some circumstances, the membrane appears to rupture by a fracture mechanism, but this effect is unusual and occurs outside the normal regime of activation [1].

Activation circuitry

An activation circuit is shown in Figure 2-5. The total circuit resistance R is divided into three parts (membrane resistance, trace resistance, and off-chip/electronics resistance) to aid in analysis and design. The membrane resistance R_{M} is strongly coupled to

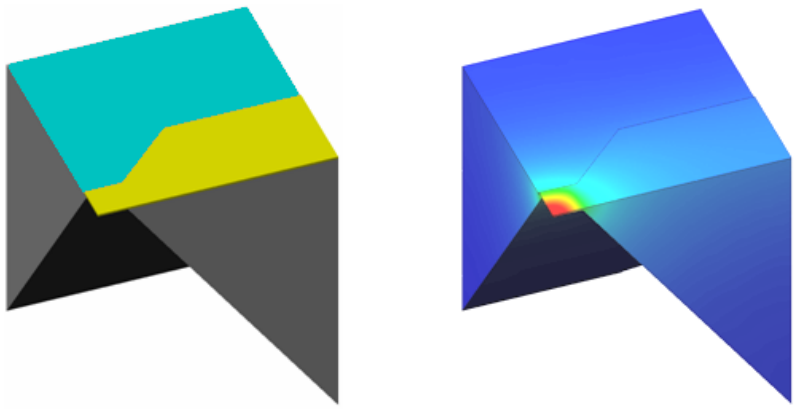

(a) (b)

Figure 2-4: Conceptual illustrations of suspended membrane as fabricated and under applied current [11].

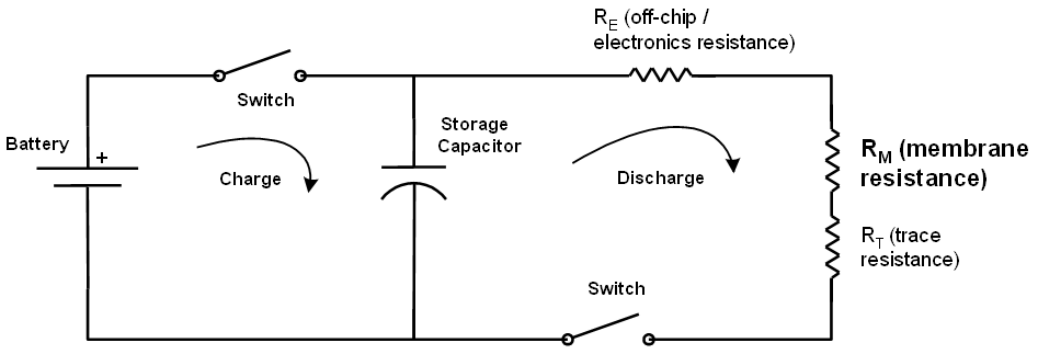

Figure 2-5: Activation circuit for electrothermal mechanism [1].

activation behavior. Only the resistive heat generated at the membrane is useful for activation; resistive heat in other components is unused and reduces efficiency. The trace resistance R_T represents the resistance of the metal patterns on the chip used to address each membrane. This value depends on the trace material, width, and thickness. The electronics resistance R_E includes the series resistance of the capacitor and switches and the resistance of all external wiring. The trace and electronics resistances typically are each approximately $1\,\Omega$ and are combined in some later analyses as the non-membrane resistance $R_{NM} = R_T + R_E$.

A suitable energy source is a capacitor with capacitance C that has been charged to a voltage V. The use of a capacitor eliminates the need for a battery to provide ampere-level activation currents. As long as the characteristic time constant RC of the circuit is much larger than the activation time (typically in the tens of microseconds), the supplied voltage can be regarded as constant during activation. This condition is not required, but it simplifies analysis and operation by ensuring that the capacitor's stored energy is not drained significantly during activation.

The switches could be mechanical, but better performance is achieved by using transistors controlled through additional circuitry. Voltages that are applied after the

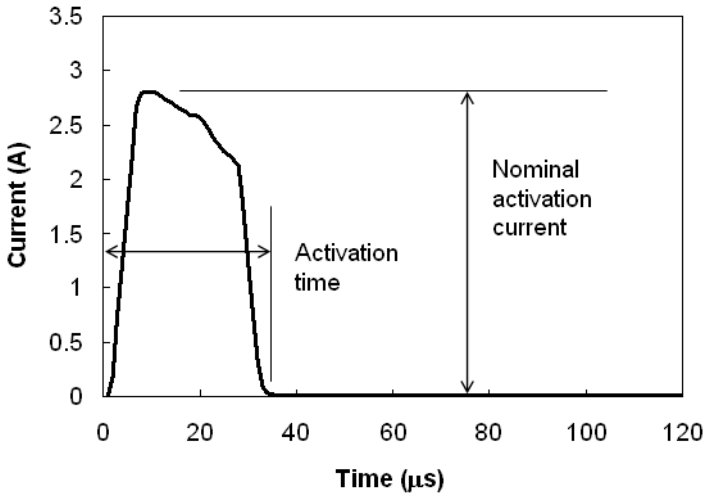

Figure 2-6: Measured activation current of a gold membrane in water [1].

circuit is broken can cause electrolysis bubbles to nucleate in the liquid surrounding the ruptured membrane area. The characteristic time of bubble nucleation has been found in experiments to be milliseconds or greater. It is therefore best for the activation pulse to be timed with a duration of less than one millisecond or for the pulse to be switched off automatically upon detection of an open circuit. The use of transistors to turn the activation current on and off enables this precise timing.

Characterization of activation

Activation can be characterized by examining the time-dependent current (Figure 2-6). This current is measured by placing a sense resistor—a low-resistance, precision resistor—in series with the circuit. The voltage drop across this resistor is then measured at a sampling rate of 1 MHz and the circuit current calculated by using Ohm's Law. Current is a suitable parameter for characterization because it is strongly coupled to the membrane's behavior as it heats and ruptures. Activation voltage, in contrast, depends not only on the membrane configuration but also on the resistance of the traces and the off-chip circuitry, and is therefore not as useful a standard of measurement.

To compare different configurations, an activation time is defined as shown in Figure 2-6. The current typically rises to a maximum value, then decreases, most likely due to the increase in membrane resistance with increased temperature and melting. Since the current changes with time, a nominal activation current is also defined to equal the ratio of the voltage V to the room temperature resistance R of the circuit. This current usually corresponds to the maximum current measured by using the sense resistor. When activation is especially rapid, however, the 1 MHz sampling rate may not be frequent enough to capture this maximum value.

Shown in Figure 2-7 are images and current measurements for gold membranes activated in water at different currents. The suspended area was $50\,\mu\text{m} \times 50\,\mu\text{m}$

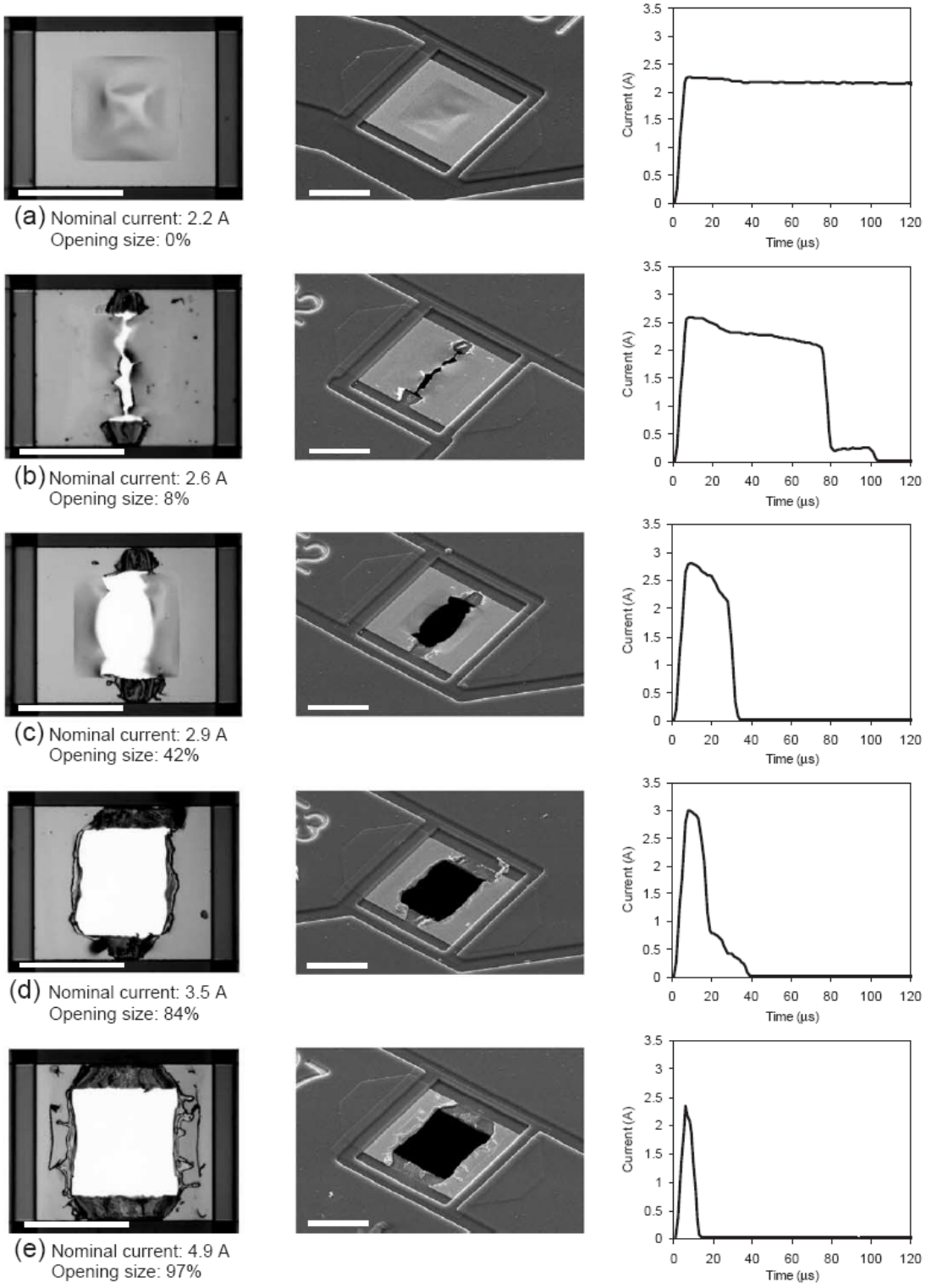

Figure 2-7: Light micrographs (left), scanning electron micrographs (center), and activation currents (right) for five gold membranes (suspended area 50 μm × 50 μm) activated in water. The scale bar represents 50 μm in all images. [1].

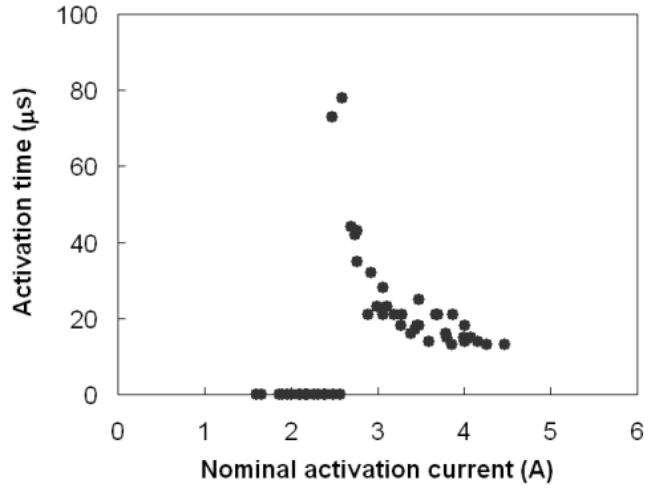

(a)

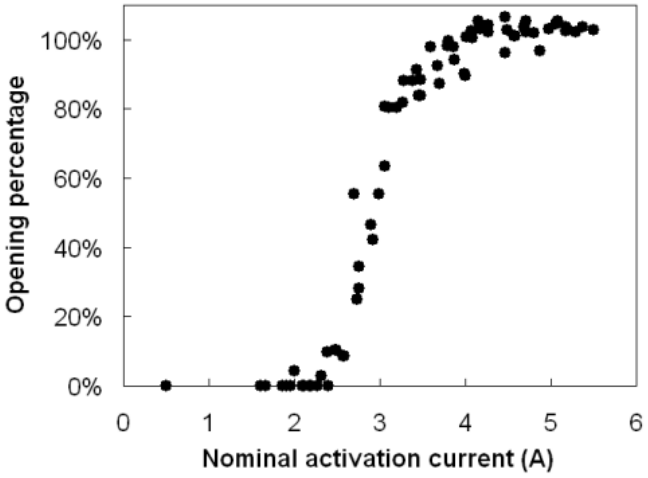

(b)

Figure 2-8: (a) Activation time and (b) opening area as a function of activation current for 50 μm × 50 μm gold membranes activated in water [1, 11].

for each membrane. The opening areas were evaluated after activation by using a calibrated optical microscope and imaging software. Note that in Figures 2-7(d,e), activation was too rapid for the data acquisition circuitry to identify the maximum current, which should equal the nominal current defined above. As the applied current increases, the activation time generally decreases and the opening size increases; these trends are plotted in Figures 2-8(a) and (b). The preferred region of activation for these devices is in the range of 4 to 5 A, where the opening size approaches 100%. A consistent large opening area is desirable because this parameter controls the flux of material in or out of the cavity, which in turn affects device performance.

Chapter 3

Materials selection

Two fabrication processes were described in the last chapter for constructing an electrothermal, controlled-exposure device. Both processes featured almost the same group of constituent materials: silicon substrates, gold traces, and titanium adhesion layers. However, there is nothing mandatory about these materials; they were selected due to constraints of biocompatibility and substrate hermeticity related to implantable drug delivery. Other applications will have different constraints.

This chapter identifies important material properties of the electrothermal device. The engineering aspects of each property are analyzed, and guidelines are generated for improving performance (for example, strengthening the device or reducing the operating current). There are always trade-offs involved in materials selection; in fact, several of the guidelines presented here directly conflict with each other. Ultimately, the process is one of optimization, where guidelines must be weighted according to the needs of the particular application.

The chapter is arranged as follows: the substrate material is addressed first, and its key properties are suggested to be its **ease of fabrication** (a term to be defined) and its **permeability**. The membrane and traces are then analyzed together with the help of an electrothermal model presented in Appendix A. The membrane material's most important properties are determined to be its **melting temperature**, **resistivity**, **thermal conductivity**, **strength**, and **hermeticity**. Resistivity is also a key property of the trace material.

An additional requirement applies to all materials and components: they must be sufficiently **stable** during fabrication and operation. That is, the materials must resist dissolution, oxidation, and any other mechanisms that would degrade device performance. In implantable applications, the stability of exposed materials is coupled to a related property, the biocompatibility of the device.

Although the focus here is on optimizing materials selection, there may be alternatives to switching materials that achieve the same result. Changing certain geometrical aspects of the device, for example, is sometimes easier than changing materials, and these alternative options are mentioned when appropriate.

3.1 Substrate materials selection

Ease of fabrication

The suitability of fabrication processes constrains the choice of candidate substrate materials (metals, semiconductors, ceramics, and polymers). How should **ease of fabrication** be defined, and which material properties would maximize it? It is useful first to consider some common fabrication methods to visualize how the device might be made for each class of material.[1] For example, cavities might be created in a metal substrate by physical methods such as punching or drilling, or the metal might be cast or electroplated in a mold. Wet chemical etching is commonly used to etch metal patterns that have been defined by masking layers. Other approaches such as electrical discharge machining, electron beam machining, and laser ablation rely on local vaporization to remove material.

Semiconductor substrates such as single-crystal silicon are commonly etched by chemical means, and various wet and dry chemical etchants allow both isotropic and anisotropic etching of silicon. An example of an isotropic etchant system is the nitric–hydrofluoric acid mixture, which oxidizes the silicon surface and subsequently dissolves the oxide. Isotropic etching tends to produce a hemispheric cavity geometry because all directions are etched at an equal rate. In contrast, some aqueous etchants such as potassium hydroxide are selective to certain silicon crystallographic planes. These solutions etch anisotropically, enabling the creation of pyramidal cavities. Dry (vapor) etching processes also come in isotropic and anisotropic flavors: xenon difluoride vapor etches silicon isotropically, while deep reactive ion etching (DRIE) combines sequential etching and passivation steps with ion bombardment to enable anisotropy and create deep trenches with near-vertical sidewalls. The chemical nature of these etchants provides relatively high selectivity and therefore allows the use of masking layers with a thickness of several micrometers or less.

Ceramics can be fired in a mold or etched by physical or chemical mechanisms. Physical etching approaches include ultrasonic drilling [18] and powder blasting [19], both batch processes. Ceramics can also be etched chemically: one example is the patterning of glass by hydrofluoric acid. DRIE has been used to etch glass, but the etch rate is relatively small (less than $1\,\mu\mathrm{m\,min^{-1}}$) because of the relative stability of Si–O bonds [20]. Masking generally becomes more difficult when physical methods, severe chemicals, or ion bombardment is required. The poor selectivity of glass DRIE, for example, limits the cavity depth to tens of micrometers even when using a metal mask several micrometers thick.

Finally, polymer substrates have been defined by molding and stamping processes, chemical etching, or curing in place. Mechanical approaches such as stamping would likely place excessive stresses on a suspended membrane, but polymers can also be etched chemically, for example by an oxygen plasma. Smigiel et al. recently reported polymer DRIE, which may emerge as a suitable method of creating cavities [21]. Alternatively, an additive photocuring approach such as stereolithography might allow

[1] Madou compares the advantages and limitations of various micromachining techniques in his textbook *Fundamentals of Microfabrication* [17].

Table 3.1: Characteristics of cavity fabrication processes for different substrate material candidates (M = metals, S = semiconductors, C = ceramics, P = polymers.)

	Commonly used for	Selective	Anisotropic	Batch
Physical processes				
Drilling, stamping	M,S,C,P	No	Yes	Some
Laser ablation	M	No	Yes	No
Powder blasting	C	No	Yes	Yes
Chemical processes				
Wet etching	M,S,C	Yes	Single crystal	Yes
Dry (vapor) etching (*e.g.*, XeF_2)	S	Yes	No	Yes
Combination phys./chem.				
Dry chemical etching w/ ion bombardment (*e.g.*, DRIE)	S	Yes	Yes	Yes
Additive				
3-D printing	M,C,P	N/A	Yes	Some
Electroplating	M	N/A	Yes	Yes
Photocuring	P	N/A	Yes	Some

the substrate to be built up around the membrane.

Selected process are evaluated in Table 3.1 according to key characteristics. It is assumed that the goal is to etch cavities in a controllable way to produce freestanding membranes. Only a few methods described above could be reasonably expected to accomplish this goal. Physical etching approaches such as drilling or powder blasting, for example, are not normally capable of stopping on a membrane of sub-micrometer thickness after removing hundreds of micrometers of substrate material. Chemical etching, in contrast, employs a chemical reaction that creates a soluble or volatile compound that is then removed. These reactions allow a high degree of selectivity and are thus favorable for fabrication.

Another desirable etching characteristic is anisotropy, which enables the creation of cavities with geometries other than hemispherical. This capability allows the creation of customized geometry such as the silicon structure shown in Figure 2-2. A third characteristic, batch fabrication, which allows simultaneous etching of cavities, is favored over sequential fabrication, especially for relatively large and dense arrays of features. Further considerations include the temperature limit of the material, the substrate's suitability for lithographic patterning, and the cost of the fabrication process.

We might therefore define ease of fabrication as the ability to successfully fabricate multiple cavities simultaneously with arbitrary geometries and capped with suspended membranes. This parameter is most strongly coupled to the nature of the cavity etching process (chemical vs. physical, isotropic vs. anisotropic, batch vs. sequential) but should also take into account the additional issues (temperature limit, suitability

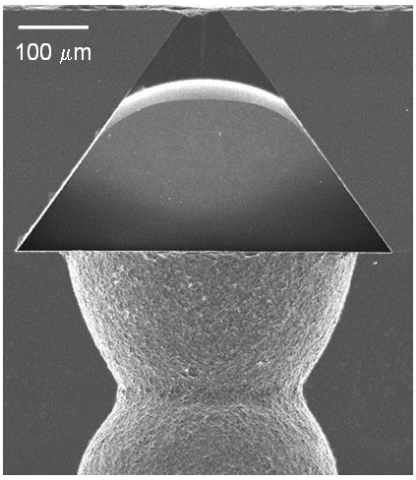

Figure 3-1: Cross-sectional micrograph of a wet-etched silicon wafer anodically bonded to a borosilicate glass wafer with powder-blasted through-wafer holes [11]. The curved feature at the top of the micrograph is the edge of an epoxy plug used to stabilize the region during sectioning.

for patterning, and cost) listed above.

Single-crystal silicon was likely chosen as a substrate for the original MIT prototypes based on considerations such as these. However, it should be recognized that alternatives exist. A single new application requirement such as optical transparency or mechanical flexibility would force a change from silicon to another material.

The discussion above presents only the broadest look at the selection of a substrate material. Exceptions exist to many of the evaluations given in Table 3.1, and new materials, tools, and techniques are always being developed to solve fabrication challenges. An example of an advanced technique is the use of combined substrate materials. In MicroCHIPS' six-month *in vivo* drug delivery study, a borosilicate glass wafer with etched through-wafer holes was added to the original silicon substrate to increase volume (Figure 2-3). A cross-section micrograph of this configuration is shown in Figure 3-1. Besides increasing volume, the glass substrate offers optical transparency, which could be useful for optical sensing applications.

Permeability

An additional constraint on candidate substrate materials is their ability to separate cavity contents from the external physical environment. Some of the degradation mechanisms of macromolecules such as proteins involve exposure to oxygen and water [22,23]. The small size and high density of the cavities make it more difficult to prevent sufficient vapor ingress to cause degradation. If the geometry and cavity contents are fixed, the only remaining parameter to alter is the substrate material's **permeability**. The permeability P is related to diffusivity D, but also incorporates the diffusing species' solubility S:

$$P = DS \tag{3.1}$$

This relationship allows transport to be estimated even if the concentration of the diffusing species in the substrate is not known; its partial pressure in the surrounding environment is sufficient. The units of permeability are $(\mathrm{cm^3\,s^{-1}})\cdot(\mathrm{cm\,cm^{-2}\,atm^{-1}})$, signifying a certain material leak rate at standard temperature and pressure ($\mathrm{cm^3\,s^{-1}}$) along a distance (cm) and across an area ($\mathrm{cm^2}$) at a certain pressure difference (atm).

The driving force for vapor ingress into a cavity is the difference in partial pressure between the external environment and the cavity. The maximum allowable permeability of a substrate can be estimated by considering the pressure difference, the sensitivity of the contents (that is, the permissible vapor pressure inside the cavity), and the cavity geometry. The relationship of interest is [24]

$$p = \Delta p_0 \left[1 - \exp\left(-\frac{PA\Delta p_0 t}{vL}\right)\right] \tag{3.2}$$

where p is the partial pressure in the cavity after time t, Δp_0 is the original pressure difference, and the associated geometry is cavity volume v, diffusion cross-sectional area A, and environment-to-cavity separation length L. Note that this analysis does not include species created by chemical reactions or desorbed from the materials inside the cavity.

As an example calculation, consider a vacuum-sealed cavity with internal volume $v = 1\,\mathrm{mm^3}$ surrounded by other cavities open to the environment, where the partial pressure of oxygen is 0.21 atm. We also assume a cross-sectional area $A = 4\,\mathrm{mm^2}$, a separation length $L = 1\,\mathrm{mm}$, and a maximum permissible oxygen partial pressure $p = 0.01$ atm. The maximum allowable permeability P is found from Equation (3.2) to be 2×10^{-11} $(\mathrm{cm^3\,s^{-1}})\cdot(\mathrm{cm\,cm^{-2}\,atm^{-1}})$. This limit is beyond the capability of most polymers. For example, nylon's oxygen permeability at 25°C is approximately 10^{-10}, polystyrene's is 10^{-8}, and silicone's is greater than 10^{-6} in the same units [25]. For larger cavities, longer diffusion distances, or less sensitive contents, however, a polymer substrate may be suitable.

The diffusion coefficient of oxygen at room temperature has been reported to be $10^{-20}\,\mathrm{cm^2\,s^{-1}}$ in silica [26] and orders of magnitude lower in silicon [27]. The oxygen permeability values would be even lower because oxygen solubility in these materials is far less than unity. Stringent permeability requirements therefore suggest the use of silicon or glass substrates over polymer substrates. A comparison of materials and the graphical calculation of suitable permeability for this example is shown in Figure 3-2.

These estimates of vapor permeation should be confirmed by experiment. Helium is typically used as a model gas because of its small molecular size and its low concentration (approximately 5 ppm) in air [24]. Helium leaks can be measured to less than $10^{-9}\,\mathrm{atm\,cm^{-3}\,s^{-1}}$ by using mass spectroscopy. However, it can be difficult to translate the helium leak rate to a corresponding water vapor leak rate. An alternate experiment for determining water vapor permeation is to enclose a hygroscopic material (a desiccant, for example) in a cavity adjacent to open cavities and to immerse the substrate in water. The water might be pressurized to accelerate the test. The

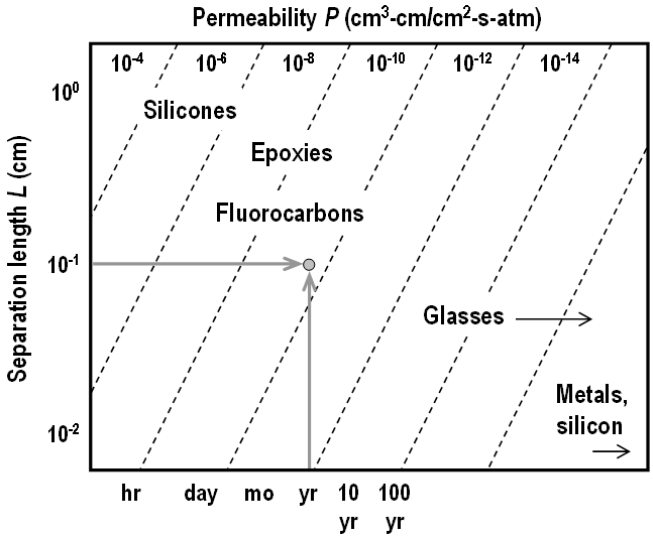

Figure 3-2: Relationship between separation length L, substrate permeability P, and time for oxygen intrusion to 0.01 atm (assumptions: initial pressure difference Δp of 0.21 atm, cross-sectional area $4L^2$, and cavity volume L^3). Data tabulated by Massey [25].

desiccant cobalt chloride changes color when hydrated, enabling easy determination of the amount of water absorbed. Water or oxygen permeation can also be estimated by sealing sensitive materials such as proteins in the cavity, exposing the substrate to the storage or operational environment for some period of time, and then removing the materials and assaying them for activity. The advantage of this test is that it measures the true parameter of interest: molecular degradation over time.

3.2 Membrane and trace materials selection

Activation-related properties

Several electrical parameters are related to activation: current, voltage, and energy, for example. Which of these should be the focus during materials selection? In fact, all of these characteristics are important at different stages of the design and testing process. The most useful measurement while testing membranes is the current, as it is the current density that controls the amount of resistive heating. The required current for a particular membrane configuration is independent of the resistance of any external circuitry, which is why the operational data in this thesis are reported in terms of current. Circuit and device designers, however, may find voltage a more useful value. The battery size is coupled to voltage, and the circuit components are all rated by voltage. Additionally, the capacitor is charged to a certain voltage that can be confirmed before activation by direct measurement. Finally, it is the amount of dissipated energy that is most strongly coupled to the temperature increase inside the cavity, and a primary function of the device is to ensure the stability of the cavity

contents. Thus, all three parameters are necessary for a complete analysis.

The first few important parameters of the membrane material are related to the electrical requirements to achieve activation. An electrothermal analysis of activation can be found in Appendix A; this analysis addresses resistive heat generation, the mechanisms of heat loss from the membrane, and the activation time and dissipated energy.

The results of the analysis in Appendix A are summarized here. First, the volumetric heat generation Q_{gen} in the membrane is found to be

$$Q_{\text{gen}} = J^2\rho = \frac{V^2\rho}{w^2(\rho + hR_{\text{NM}})^2} \tag{3.3}$$

where J is the current density, ρ is the membrane electrical resistivity, V is the activation voltage, w is the width of the membrane feature (including the overlap of the membrane over the substrate), h is the membrane thickness, and R_{NM} is the non-membrane resistance. This relationship suggests that heat generation can be maximized by adjusting the **resistivity** of both the traces and the membrane. The trace material resistivity should be minimized to reduce the non-membrane resistance as much as possible: low-resistivity materials such as silver, copper, gold, and aluminum are the most suitable. If the trace material is otherwise constrained, an alternative is to increase the width or thickness of the traces or to reduce the resistance of the other circuit components.

The membrane resistivity is optimized by selecting a value equal to hR_{NM} to maximize the power transfer from the energy source to the membrane. Either the membrane material could be changed or an impurity added to the existing material to increase resistivity. The effects of alloying on metal resistivity are shown in Figure 3-3. Resistivity in metals increases with small concentrations of an impurity, as seen in Figure 3-3(a). Further increasing the concentration eventually again reduces the resistivity as the impurity becomes the dominant element (Figure 3-3(b)) or as ordered intermetallics form (Figure 3-3(c)). As alternatives to changing the material, the resistance of the membrane might also be altered by changing its thickness or by changing its length-to-width ratio.

The second result of Appendix A involves heat loss from the membrane, which is desirably minimized. Heat loss is dependent in part on the temperature increase in the membrane. For example, conduction through the membrane and conduction to the surrounding environment are proportional to the temperature rise $\Delta T = T - T_\infty$, where T_∞ is the ambient temperature. Radiative heat loss is proportional to the difference of the fourth power of temperature ($T^4 - T_\infty^4$). Boiling is associated with significant values of heat flux due to the energy associated with a phase change. The next guideline is therefore to reduce the material's **melting temperature** to as low a value as possible. The melting temperatures of MicroCHIPS' membranes are relatively high: gold melts at approximately 1060°C, titanium at 1670°C. How were these materials selected? The electrochemical mechanism used gold membranes because gold can be electrochemically dissolved in saline, and the electrothermal concept was first demonstrated by using microchips configured for the electrochemical method.

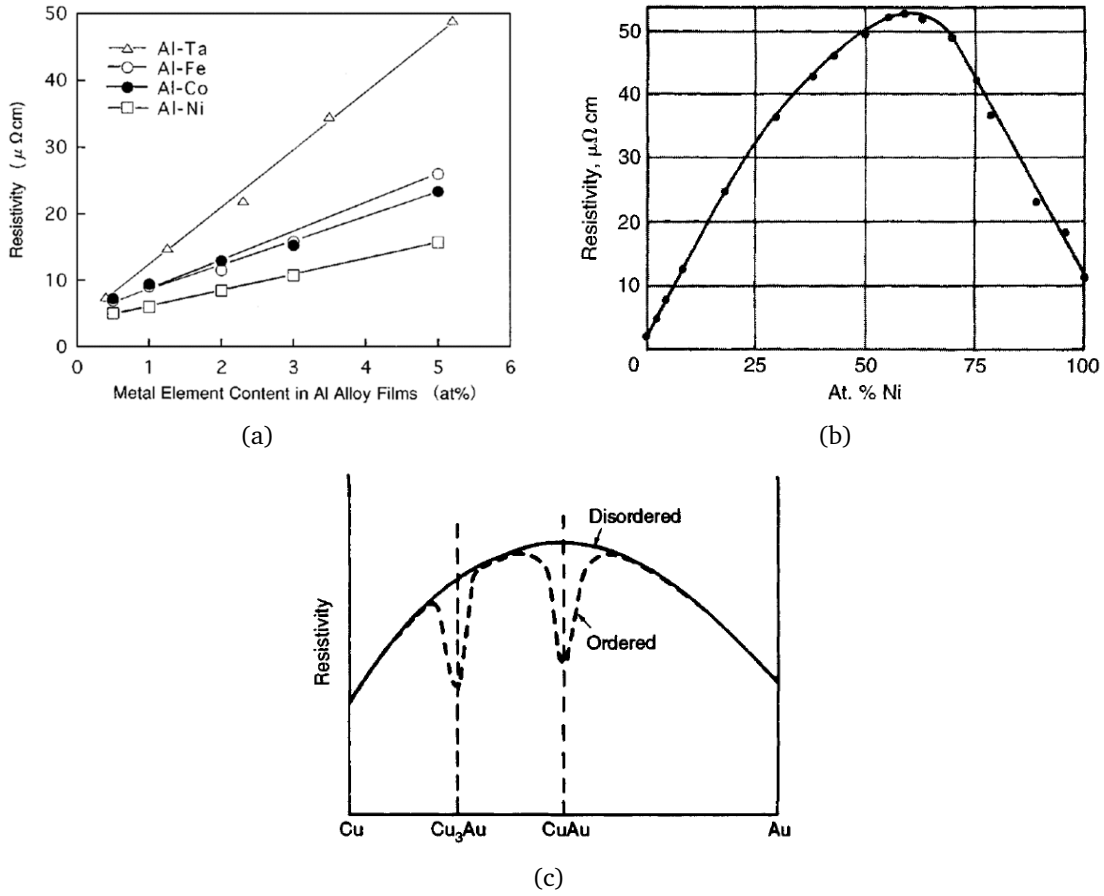

Figure 3-3: (a) Resistivity of aluminum-containing films as a function of alloying element content [28], (b) Resistivity of copper-nickel films as a function of nickel content [29], and (c) Resistivity of copper–gold films as a function of gold content [30].

Titanium membranes were later introduced by applying the guideline above addressing membrane resistivity: titanium, whose resistivity is an order of magnitude larger than that of gold, was selected to increase the membrane resistance R_{M} to the same magnitude as the non-membrane resistance R_{NM}. Considerations of biocompatibility also influenced the selection of both materials.

We might consider using a membrane material whose melting temperature is much closer to ambient temperature, ideally below the boiling point of water to eliminate boiling-related losses.[2] Indium, which melts at 157°C, is one possibility. An alloy of indium and tin might also be used; the phase diagram of this system is shown in Figure 3-4. This system features a eutectic, a melting point lower than that of either of the constituent metals, when the elements are combined in approximately equal parts.

[2]The melting temperature need not be lower than 100°C, however, to prevent boiling. Boiling temperatures are larger in the case of a rapid temperature increase on smooth surfaces because of the energy penalty of nucleating a vapor bubble. The boiling temperature of water on smooth surfaces at large heating rates has been theoretically estimated and experimentally found to be larger than 300°C [31–33].

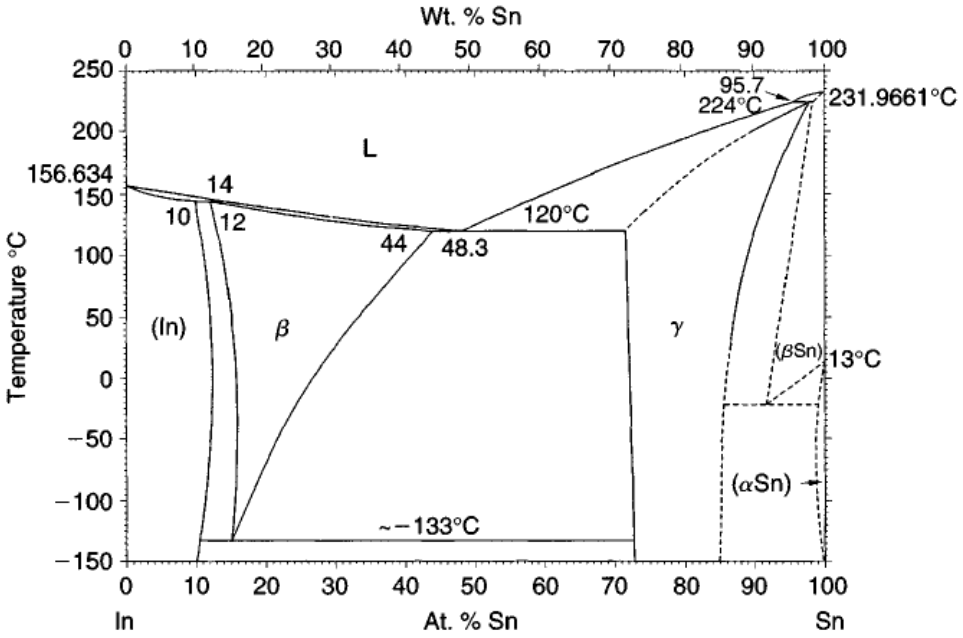

Figure 3-4: Indium-tin phase diagram [29].

Alloying may also have a favorable influence on strength and hermeticity, as described later in this chapter. Alloy deposition could be accomplished by cosputtering, in which two separate targets are sputtered at independent power levels to enable arbitrary film stoichiometry. Another approach is to cast an alloy target from which the film is sputtered; this approach is well suited for the manufacturing stage after an alloy composition is selected.

The third relation from Appendix A applies specifically in the case where heat conduction through the membrane is the dominant mechanism of heat loss. This situation is more likely when the membrane size (width and length) is small, the thickness h is large, or the thermal conductivity k of the membrane material is large. Under these conditions, the following estimate for required voltage V_{req} applies:

$$V_{\text{req}} = 2(\rho + hR_{\text{NM}})\sqrt{\frac{k\Delta T}{\rho}} \tag{3.4}$$

where k is the membrane thermal conductivity and ΔT is the temperature difference between the center and the edge of the membrane. Note that the guidelines of optimizing ρ and reducing ΔT are still valid in Equation (3.4). Additionally, a material with a lower **thermal conductivity** could be used to reduce the required voltage. At a certain point, however, the conduction term will no longer dominate and the analysis above will no longer be valid. The membrane thickness h could also be reduced, with the same condition that this optimization step tends to suppress the circumstances under which it applies.

It is also important to note that electrical resistivity and thermal conductivity are inversely related in metals. This relationship is described by the Weidemann-Franz

Law: the ratio $k\rho/T$ is approximately equal to a constant ($2.45\times10^{-8}\,\mathrm{W\,\Omega\,K^{-2}}$). The thermal conductivity of a metal is therefore also affected by alloying.

The fourth result from Appendix A is that lower bound of energy dissipated $E_{\mathrm{M,min}}$ is given by

$$E_{\mathrm{M,min}} \approx 4r_0^2 hp(c\Delta T + H_{\mathrm{m}}) \tag{3.5}$$

where r_0 is half the side length of the membrane, c is the membrane specific heat, p is the membrane density, and H_{m} is the membrane material's heat of melting. This lower bound is the amount of energy needed to heat the membrane to its melting point and to melt it. Reducing the dissipated energy toward this minimum value requires the activation voltage and current to be increased.[3] It may be advantageous in some applications to minimize the energy in this way. So far, however, the strategy for operation has been to use the minimum voltage that ensures consistent operation; this strategy is driven mainly by the desire to reduce the battery size of the implantable device in *in vivo* applications.

Strength

The microchip's usefulness is compromised if the membranes are too fragile to withstand loading conditions during fabrication, handling and shipping, and operation. There is therefore an interest in increasing membrane **strength**. In general, the membranes can withstand relatively large pressures, but are susceptible to damage from small displacements. For example, 0.3 to 0.4 μm thick, 50 μm × 50 μm Pt/Ti/Pt membranes have been found to be resistant to rupture at fluid pressures of up to tens of atmospheres. A displacement of only one micrometer, however, applied near the connection point between the membrane and the substrate would likely shear the membrane and create a leak path.

The strength of thin films is known to depend on the thickness. For example, Espinosa et al. found that the yield strength of evaporated gold is independent of thickness for columnar-grained films, but drops by almost 50% for films that are more than one or two grains thick [35]. This transition occurred at a thickness between 0.5 and 1.0 μm and was attributed to the increased number of slip systems in the thicker films. The dependence of yield strength on thickness complicates the process of designing membranes for a particular strength. It is usually necessary during the design process to suuplement theoretical calculations with rupture tests of actual films.

Stronger membrane materials are desirable because they would enable the successful fabrication and use of larger membranes, which expose more area. However, metals with lower melting temperatures tend to have lower yield strengths, and problems involving membrane strength may arise with the incorporation of new membrane materials for reduced current.

[3] This guideline is somewhat counterintuitive but is supported by theoretical and experimental results (Equation (A.12) and Figure A-5, respectively). Higher currents and voltages accelerate the activation process and reduce the concomitant heat loss from the membrane to the surrounding environment.

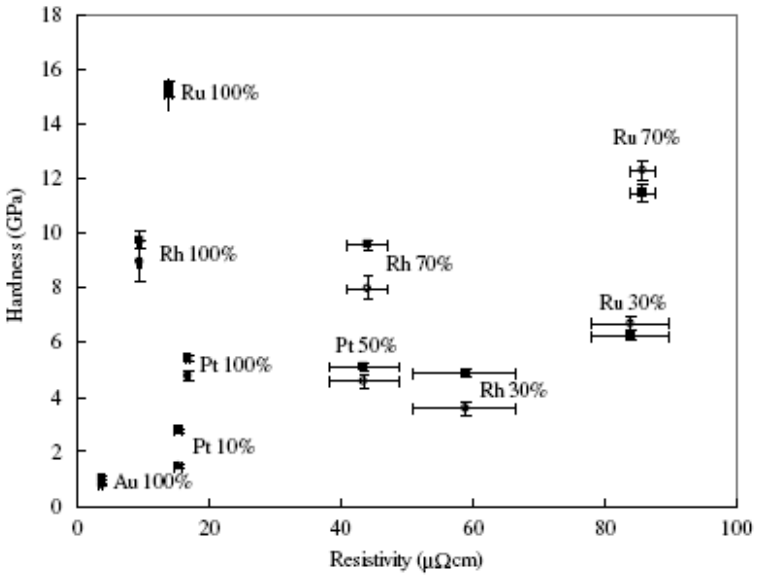

Figure 3-5: Hardness and resistivity for different gold-containing alloys [34].

One approach to strengthening bulk metals is to use an alloy, and this approach could be applied to the membrane as well. Solid solution alloying increases yield strength because the strain field of each solute atom interacts with the dislocation strain field and hinders dislocation motion [36]. Alloying has been demonstrated as a way of strengthening microfabricated features. Brazzle et al., for example, strengthened platinum flexures for micromirrors by alloying with iridium (10%) and also with ruthenium and rhodium (6% and 15%, respectively) [37]. The features were deposited by sputtering from a cast target. The yield stress of these alloys was determined to be greater than 1 GPa. Additionally, Lee et al. added platinum, rhodium, and ruthenium to gold films to strengthen microscale electrical contacts and compared the hardness and resistivity of the alloys (Figure 3-5) [34].

Membrane survival is also promoted by gentle handling: contacting the membrane with smooth surfaces only and avoiding direct rinsing sprays. The environment in envisioned *in vitro* applications is a relatively gentle sample stream that is not expected to rupture the membranes. For *in vivo* applications, it is desirable to place the membrane in contact with smooth tissue only. The best geometry seems to be multiple smaller membranes per cavity, as described by Santini et al. [15]. Cima et al. have also described reinforcing strips over the membrane that are intended to provide a similar strengthening effect [38].

Hermeticity

The membrane should be sufficiently **hermetic** to prevent degradation of the contents of the cavity before it is opened. Protein stability is strongly dependent on the storage environment, especially the surrounding moisture and oxygen content [22,23]. Moisture and oxygen ingress through the membrane can occur in several ways.

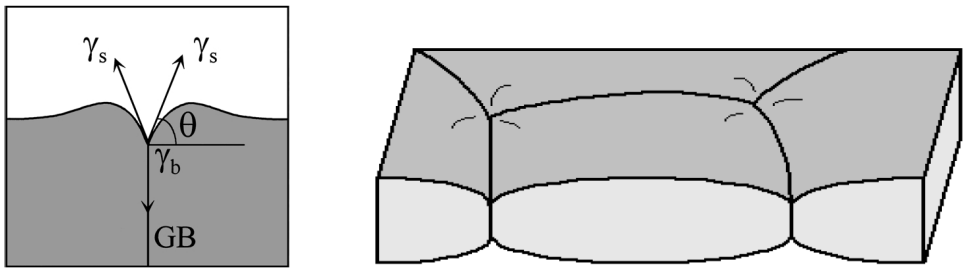

Figure 3-6: Illustration of thermal grooving and triple junctions in a suspended thin film [43].

First, pinhole defects may appear during membrane deposition. This problem was observed with prototypes fabricated at MIT's Microsystems Technology Laboratories (MTL) in which e-beam evaporation was used to deposit the membrane. Tsau at al. independently reported the same problem at MTL after depositing gold films for a different application; they attributed the cause to source spitting from the evaporation crucible [39]. Pinholes have not been observed in membranes that have been deposited by sputtering, however, and the problem of large defects has essentially disappeared in current MicroCHIPS devices. The most likely reason is that sputtering does not involve molten material and is not susceptible to source spitting. Additionally, sputtering produces a conformal coating that may cover impurity particles better than evaporation.

The second mechanism is pinhole nucleation. Surface grooves can appear in a film along the paths where grain boundaries intersect the surface (Figure 3-6). The driving force is the reduction of surface area [40]. The process tends to reduce film thickness; in a suspended film, the effect occurs on both sides and can result in pinholes nucleating at the so-called triple junctions where three grains meet.

Pinhole formation is a diffusion-related process and is strongly dependent on the film temperature. Suspended gold films, for example, are susceptible to pinhole formation in minutes at temperatures greater than 500°C [4]. The self-diffusivity of metals is roughly equal at the homologous temperature (T/T_{m}, where T_{m} is the melting temperature) [41]. As a result, self-diffusion effects are more significant for metals with lower melting temperatures. However, there is some evidence of grooving suppression by alloying [42]; furthermore, small amounts of impurities are known to be capable of suppressing recrystallization, another diffusion process [36]. Alloying may therefore be a useful way to address pinhole formation in low-melting-temperature membrane materials.

The third type of leak is atomic or molecular diffusion through grains or (more likely) grain boundaries. Grain boundaries are known to be relatively easy diffusion paths due to their increased atomic spacing. Diffusion will be strongly dependent on the method of deposition and the nature and concentration of impurities in the films, which will tend to segregate at grain boundaries. In practice, the helium leak rate through suspended metal membranes has been found to be less than 10^{-9} atm cm^{-3} s^{-1}

[13], and this value is thought to be sufficiently low to prevent degradation in typical controlled-exposure applications.

3.3 Selection of materials for device stability

A final requirement is that all materials should be stable in and compatible with the intended working environment. Stability here involves the possibility of corrosion, dissolution, or other degradation mechanisms. Compatibility involves the possibility for degradation products to negatively impact the system.

The literature on biostability and biocompatibility is large. A general approach to ensuring device stability it to make it thermodynamically or kinetically unfavorable for the device to degrade. For example, the platinum coating on Pt/Ti/Pt membranes is resistant to forming soluble complexes in liquid. The titanium would fully oxidize over time, but oxidation is kinetically restricted both by the existing native oxide layer and the platinum coating.

Stability can be investigated in several ways. The material or device can actually be implanted, and this method gives the most valid results. It is also the most expensive. The material can be immersed in a simulated physiological medium at 37°C and examined periodically. This approach results in more uncertainty than the implantation approach, since the medium cannot replicate complex activity such as inflammation (although known components of the inflammation response, such as increased hydrogen peroxide, can be added to the mixture). It also occurs in real time. A third approach is accelerated testing, in which the activity of the degrading medium is increased either by increasing temperature or by adding more concentrated solutes. This technique provides data the most rapidly. A disadvantage is that other modes of degradation might be activated that would not be expected to occur in normal operation.

Compatibility, the impact of the material on the environment, can also be evaluated at different levels of realism. For *in vitro* applications, the contents of the cavity and the sample stream can be exposed to the device and changes in operation measured. For *in vivo* applications, the device might be placed in a cell culture or implanted in an animal to determine the degree of inflammation or to estimate the risk of more severe responses.

Chapter 4

Commercialization

There are multiple ways to position any new technology in the marketplace. Santini et al.'s first prototypes, which operated by the electrochemical mechanism, were conceived as precursors to a "pharmacy-on-a-chip," and the focus was on controlled release and medical implantation [5]. At MicroCHIPS, this focus has since shifted to the more general concept of controlled exposure. Santini recently described the electrothermal mechanism as a "smart package" that might release chemicals, expose sensors, or both [13].

Commercialization of the electrothermal technology is investigated in this chapter. The advantages and limitations of the technology are first reviewed, and the area of sensor exposure is chosen for investigation. Two applications, biowarfare agent detection and *in vivo* glucose sensing, involve frequent or continuous sensing, but progress in these areas is limited by sensor lifetime. A controlled-exposure technology would address the problem by enabling the periodic exposure of fresh sensors. Incorporation of this technology with existing sensors could provide revenue through a partnership with sensor companies and the sale of augmented devices.

4.1 Identifying favorable applications

Several questions are useful in identifying an appropriate application or market for a new technology:

1. **What are the capabilities and limitations of the new technology?** Although it is more common to compare concepts by their respective strengths, it is useful to also explore the constraints and eliminate applications where the constraints are the limiting factor. For example, the relatively small capacity (<1 μL) of Santini et al.'s controlled-release microchips has led MicroCHIPS to investigate the *in vivo* release of only the most potent compounds [4].

2. **In what applications is the technology necessary?** However interesting or clever the concept, success in the marketplace depends on providing an added value sufficient to justify expense.

3. **Is the market lucrative?** Alternatively, is the market prominent? The application of any new technology desirably leads to a large revenue stream. However, a prominent application involving a long-sought-after goal could also be favorable if it attracts public attention and more investors.

4. **How would value be extracted?** A business model necessarily includes a strategy for how money will be made when the technology is introduced into the marketplace.

The first question, involving advantages and limitations, can be addressed immediately. The rest of this chapter addresses the remaining questions for the applications that emerge as most favorable.

Capabilities and limitations

The electrothermal mechanism has the following general capabilities and characteristics:

- Hermetic long-term storage of material in solid, liquid, or gel form.
- Large arrays of discrete cavities containing a variety of contents.
- Exposure on command of drugs, sensors, cells, or other contents, or a combination of these.
- Automated, closed-loop system regulation.

A number of limitations are apparent, however:

- Cavity contents cannot be changed after the sealing process, and the device cannot be reused after the membranes are ruptured. Exposure is thus limited to one-time use only; the device is not a hermetic valve.
- Membranes are individually addressed, making the device difficult to access electrically when large arrays of cavities are fabricated.
- The instantaneous current requirement of 1 A or more is challenging to supply in some applications such as medical implantation. The power requirements are strongly coupled to the membrane material, which may be constrained by strength, hermeticity, and stability requirements.
- The $<1\ \mu$L payload limits the number of possible dispensing applications. The payload could be increased by increasing the substrate thickness at the cost of increasing the required diffusion length, characteristic release time, and device size.
- The technology at this point costs more than mature dispensing methods (such as microsyringes) and mature manual-exposure methods (such as blister packs).

- The food and drug administration (FDA) has not (yet) approved this technology for use.

The drug delivery application was discussed in a previous MEng thesis [14], and is not discussed further here. Instead, the applications addressed in this chapter involve the controlled exposure of sensors. The packaging of sensors removes some limitations: payload volume is no longer a significant constraint, for example. Additionally, the one-time exposure capability is well suited for periodic exposure of fresh sensors.

It remains to be determined whether the value of storing and periodically exposing sensors justifies the cost of incorporation. The most favorable markets are identified by looking at applications where frequent or continuous sensing is important (for example, for national security reasons or for avoiding health problems) but where current sensing strategies are limited by sensor lifetime. The two areas examined here, biowarfare agent detection and *in vivo* glucose sensing, were chosen to fulfill these criteria.

Sensing mechanisms and signal generation

The second question in the commercialization checklist above concerns the need for the technology and the most suitable uses for the mechanism. Before discussing applications in detail, it is first useful to identify which sensing mechanisms are appropriate for packaging in an array and exposing in a controlled manner. For example, electrochemical sensors are well suited for miniaturization; these sensors operate by measuring the voltage, current, or impedance between electrodes. Optical sensors rely on a change in optical properties of a substrate, film, or fluid due to the presence of the species of interest. One detection method, for example, consists of measuring fluorescence intensity by photodiodes. Even though it may not be practical to package multiple photodiodes in cavities, a single photodiode array underneath a transparent substrate could interrogate different areas of the substrate as they are exposed. Finally, microfabricated structures such as cantilevers or membranes may deflect or exhibit a change in dynamic response due to surface binding of molecules. The response can be measured electrostatically or piezoelectrically, and the whole assembly could be packaged and controllably exposed.

The mechanisms described above are at least one step removed from actual sensing of an analyte; they are not yet selective to the species of interest. Selectivity is enabled by adding a molecular recognition element to the sensor. One example can be found in the electrochemical approach of measuring lactose *in vivo* by amperometry. One of the electrodes is maintained at a potential of approximately $+0.7\,\mathrm{V}$ (vs. a Ag/AgCl reference electrode) to oxidize hydrogen peroxide in the vicinity, and the resulting faradaic current is measured. A layer of lactose oxidase over this electrode provides selectivity by catalyzing the oxidation of lactose while simultaneously producing hydrogen peroxide. Another example is the deflection of a membrane due to surface binding of molecules. Selectivity is achieved here by coating the membrane with bound antibody molecules that have an affinity to one particular antigen that (in theory) will then be detected over all others.

Why is it necessary to periodically expose fresh sensors? A common limitation is that the molecules and layers that provide selectivity are susceptible to degradation. For example, enzyme proteins may degrade in the presence of oxygen, hydrogen peroxide, water vapor, or other environmental factors. Additionally, the sensor may be fouled with background or contaminant material, blocking the detection of the analyte of interest. The outcome of these degradation phenomena is a general need for periodic exposure of new sensor surfaces.

4.2 Biowarfare agent detection

One commercialization strategy is to select candidate markets in which continuous sensing would be valuable but is currently impossible or impractical. The first area of interest is the exposure of sensors for biowarfare agent detection. Continuous sensing is desirable in this area for public health and national security reasons but is challenging because of sensor lifetime limitations.

A 2003 National Defense University report describes the motivation behind detection:

> The 21st century opened with the startling use of anthrax spread deliberately through the United States mail system, resulting in 5 dead, at least 17 infected, and more than 30,000 on preventative antibiotics. It also led to substantial disruptions in normal activities, the revision of long-standing procedures, and the expenditure of several billion dollars for decontamination efforts. At present, the intelligence community assesses that "approximately" a dozen states maintain offensive [biowarfare] programs and that interest among particular subnational organizations is high... **Protecting United States forces, facilities, and civilians at home and abroad from biological weapons is a pressing national priority.** [44] (emphasis added)

Biowarfare agents can consist of bacteria, toxins, or viruses. The Centers for Disease Control (CDC) classifies these agents as follows (Table 4.1):

> [Category A diseases/agents] include organisms that pose a risk to national security because they can be easily disseminated or transmitted from person to person, result in high mortality rates and have the potential for major public health impact, might cause public panic and social disruption, and require special action for public health preparedness. [Category B diseases/agents] include those that are moderately easy to disseminate, result in moderate morbidity rates and low mortality rates, and require specific enhancements of CDC's diagnostic capacity and enhanced disease surveillance. [Category C diseases/agents] include emerging pathogens that could be engineered for mass dissemination in the future because of availability, ease of production and dissemination, and potential for high morbidity and mortality rates and major health impact. [45]

Methods of detecting toxic warfare agents include tools such as mass spectrometry, polymerase chain reaction (PCR), and antibody- and enzyme-based sensing. The

Table 4.1: Centers for Disease Control (CDC) list and classification of biological threat agents [45, 46]. Agent type: B = bacterium, T = toxin, V = virus.

Disease (organism)	Agent type
Category A	
Anthrax (*Bacillus anthracis*)	B
Botulism (*Clostridium botulinum* toxin)	T
Plague (*Yersinia pestis*)	B
Smallpox (variola major)	V
Tularemia (*Francisella tularensis*)	B
Viral hemorrhagic fevers (filoviruses [*e.g.*, Ebola and Marburg] and arenaviruses [*e.g.*, Lassa and Machupo])	V
Category B	
Brucellosis (*Brucella* species)	B
Epsilon toxin (from *Clostridium perfringens*)	T
Food safety threats (*e.g.*, *Salmonella* species, *Escherichia coli* O157:H7, *Shigella*)	B
Glanders (*Burkholderia mallei*)	B
Melioidosis (*Burkholderia pseudomallei*)	B
Psittacosis (*Chlamydia psittaci*)	B
Q fever (*Coxiella burnetii*)	B
Ricin toxin (from *Ricinus communis* [castor beans])	T
Staphylococcal enterotoxin B	T
Typhus fever (*Rickettsia prowazekii*)	B
Viral encephalitis (alphaviruses such as Venezuelan equine encephalitis, eastern/western equine encephalitis)	V
Water safety threats (*e.g.*, *Vibrio cholerae*, *Cryptosporidium parvum*)	B
Category C	
Emerging infectious diseases such as Nipah virus and hantavirus	V

characteristics and use of these tools have been reviewed by Paddle [47], Iqbal et al. [48], Lim et al. [49], and Gooding [50]. This section focuses on one specific class of sensor as an exemplary candidate for packaging and exposure: optical sensors employing antibodies for molecular recognition. There are several advantages to this selection. First, multiple surface areas with bound antibodies can be selectively exposed and interrogated by optical components. Second, optical sensors may be cheap enough that multiple devices (each including an array of packaged surfaces) could be manufactured for distributed or handheld sensing. This concept has been described in a 2004 report by the National Research Council of the National Academies:

> Chemical sensors are versatile and available in many configurations that can be small in size, rapid in reporting information, and low in cost. If such sensors could be made reliable enough and cheap enough, it might be possible to use them as biological “smoke detectors” and distribute them widely throughout a building or

> other target that needs to be protected. When highly distributed, they are likely to be closer to any potential release and hence experience a still larger concentration of agent, thereby possibly lessening the stringent demands on discriminating an agent from the ambient background. It is this interplay of highly distributed and cheaper but simpler sensors that offers an intriguing trade space. [46]

Third, antibody-based optical sensors are already in use, and it should be possible to package antibody arrays without significant modification. This ease of integration makes a partnership with a sensor manufacturer more practical from a business perspective than if it were necessary to develop and characterize a new sensing mechanism.

Optical antibody-based detection

Antibody-based sensors rely on molecular recognition and binding between antibodies (which are provided with the sensor) and antigens (which are sensed in the sample stream). These sensors provide relatively high sensitivity (parts per billion or better [50]). Along with this sensitivity, however, comes a problem of reversibility. Since molecular binding is so favored thermodynamically that unbinding is rare, sensors cannot be re-used and usable sensor lifetime is limited. This factor motivates the use of a controlled-exposure mechanism: the more irreversible the reaction, the more sensitive the sensor, and also the more necessary the controlled-exposure capability for periodically exposing new sensor surfaces.

Some relevant optical sensors demonstrated in the literature are listed here. The following devices are candidates for integration with a controlled-exposure mechanism:

- The Autonomous Pathogen Detection System (APDS) was developed at Lawrence Livermore National Laboratories for detection of biowarfare agents [51, 52]. An aerosol cyclone collector first transports particles into a liquid sample.[1] The system then periodically performs an antibody-based assay and initiates polymerase chain reaction (PCR) amplification if an analyte of interest is detected. A flow chart for operation is shown in Figure 4-1(a). The device was reported to operate for seven days, performing 154 assays. A number of pathogens, including *Bacillus anthracis*, *Yersinia pestis*, *Bacillus globigii* (a *Bacillus anthracis* simulant), and botulinum toxoid (inactivated botulinum toxin) were successfully detected (Figure 4-1(b,c)) [52].

[1] Sample collection is a complicating factor when detecting harmful particles in air. Bacterial spores are not associated with any significant vapor pressure, and it is necessary to sample large quantities of air (several hundred liters or more) per diagnostic step. Collection methods have been developed to convert these spores into a liquid environment [53]. For example, cyclone samplers and virtual impactors are two tools that operate by an inertial mechanism, in which particles are separated by size and diverted into a liquid. Another approach is bubbling, in which aerosols are sprayed into a liquid, which is then assayed. Particle collection devices may also incorporate a trigger that checks particle sizes and initiates a sensing sequence if a significant increase in particle count is detected.

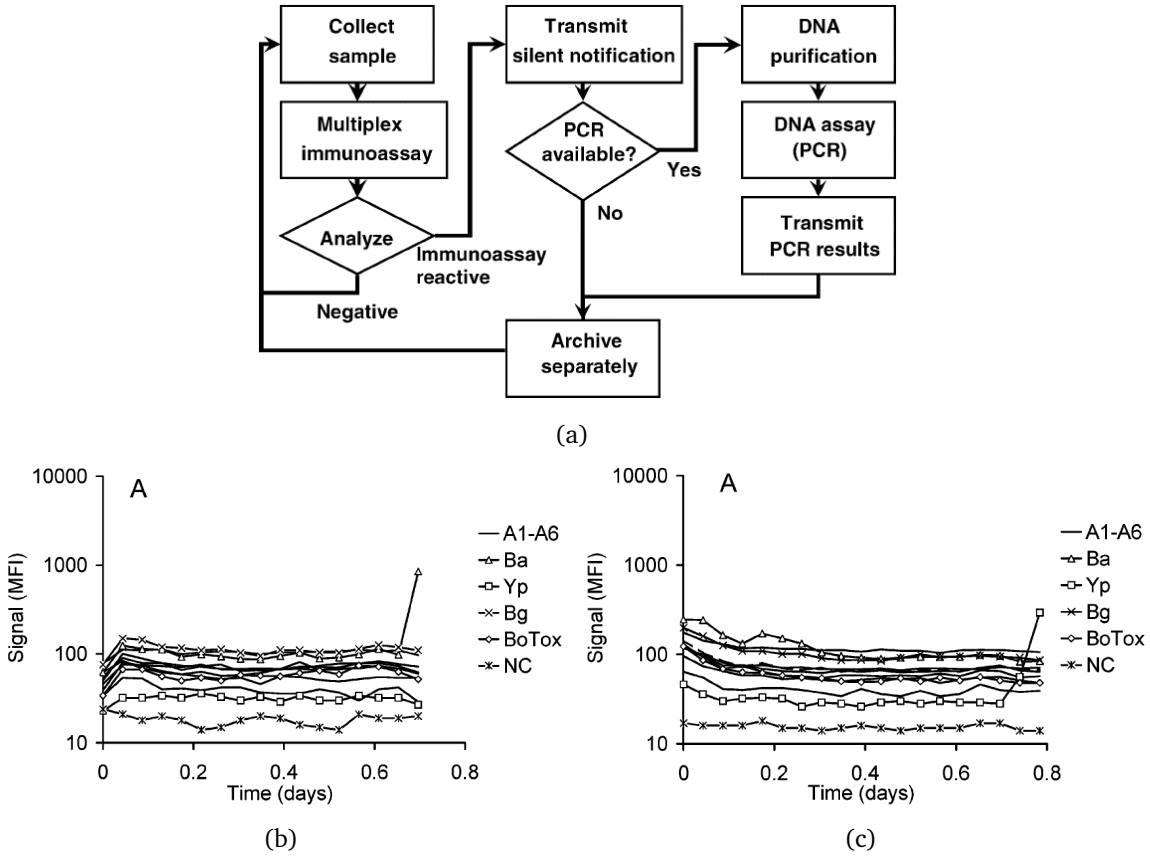

Figure 4-1: (a) Flow chart for Autonomous Pathogen Detection System operation; (b,c) Antibody-based detection of anthrax (Ba = *Bacillus anthracis*) and plague (Yp = *Yersinia pestis*) (MFI = median fluorescence intensity) [52].

- Naimushin et al. attached an antibody-based sensor to an aircraft acting as a surrogate unmanned aerial vehicle [54]. The device employed a detection mechanism known as surface plasmon resonance (SPR), which is described later in this chapter. Ovalbumin and horseradish peroxidase acted as biowarfare agent simulants, and samples were collected by a gravity droplet collector. The sensor successfully detected the analytes.

- Rubina et al. demonstrated the detection of several of the agents in Table 4.1 (anthrax, ricin, and staphylococcal enterotoxin B) on a single substrate by using a fluorescence immunoassay (Figure 4-2) [55].

The devices described above demonstrate that optical antibody-based assays are available for detecting the CDC's species of interest and that detection is feasible in real applications such as airborne detection of particles. Additionally, multiple analytes can be detected on a single substrate. However, a significant challenge involves the usable lifetime of sensor surfaces. The 2004 National Academies report emphasizes the difficulty with sensor surface replacement or regeneration in continuous monitoring:

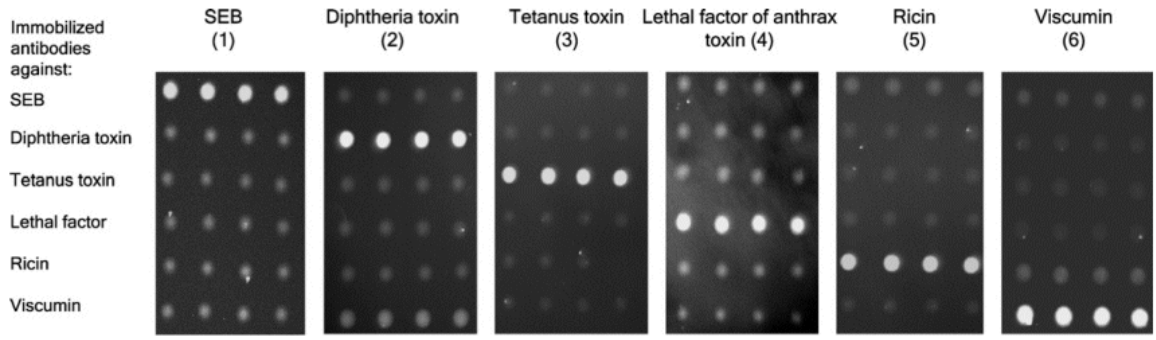

Figure 4-2: Antibody-based detection of multiple biowarfare agents on a single substrate developed by Rubina et al. [55].

> For continuous use of a sensor, [the sensor surface must be regenerated] at the end of an analysis. This is sometimes achieved by changing the wash conditions to disrupt the interaction between the target and the molecular recognition element. The stringent washing must remove bound target and nonspecifically bound materials but leave the molecular recognition element unaffected. **Renewal of the sensor surface is typically only possible for a limited number of cycles, after which time the sensor surface must be replaced due to degradation.** [46] (emphasis added)

The same report discusses the need to expose new sensor surfaces:

> Two important considerations for extended sensor operation and environmental monitoring are reversibility of the binding interaction and surface fouling... [H]arsh conditions can affect the quality of the interactive surface and therefore limit the lifetime of the sensor... Surface fouling can result in false positive signals or completely destroy the operation of the sensor by interfering with analyte-sensing surface interactions, giving false negative signals... **If continuous or periodic monitoring over extended periods of time is desired, it is often necessary to engineer the sensor system to produce a new sensing surface automatically for each measurement, or to replace the sensing surface periodically as surface fouling occurs.** [46] (emphasis added)

These comments indicate that there is sufficient motivation to integrate a sensor device that can be fabricated in an array configuration with a technology for controlled exposure.

Integration of controlled-exposure technology

A concept for controlled exposure of an optical sensor is illustrated in Figure 4-3. This particular sensor operates by surface plasmon resonance (SPR), the mechanism used by Naimushin et al. for airborne detection [54]. An SPR sensor detects a molecular binding event by reflecting light off of a thin metal film on which antibodies are

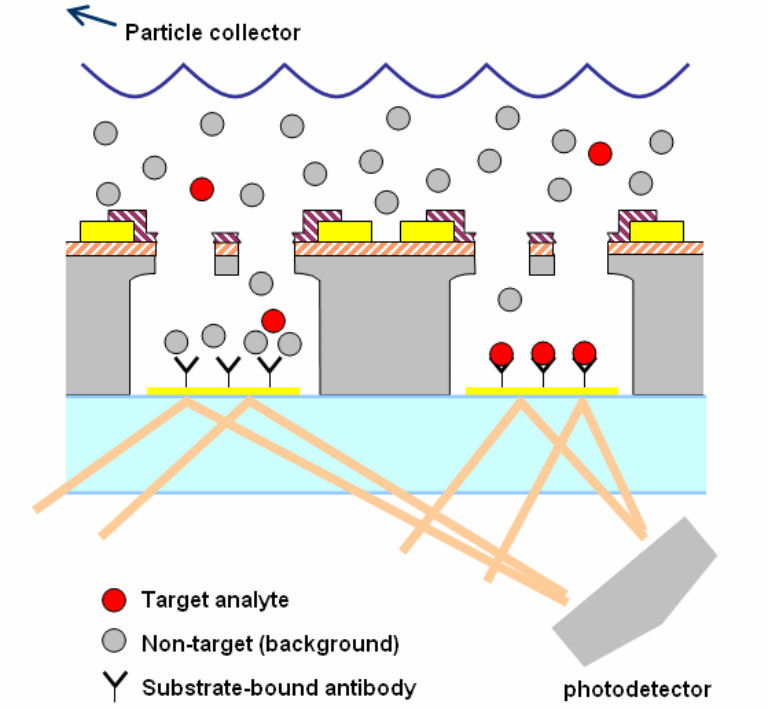

Figure 4-3: Schematic of multiple antibody-coated surfaces exposed by the electrothermal mechanism and optically monitored. The sensor exposed first (left) may not detect the analyte of interest due to fouling from adsorbed or deposited background molecules. The newly exposed sensor (right) successfully detects the analyte.

bound. The technology is described in a North American Technology and Industrial Base Organization report:

> SPR is a quantum effect arising from the interaction of light reflecting from a metal surface. Under certain conditions, the energy carried by photons of light is transferred to packets of electrons, called plasmons, on a metal surface. Energy transfer occurs only at a specific resonance wavelength of the incident light, and the resultant effect is absorption of the light at this resonance wavelength. The SPR resonance wavelength is determined by three factors: the metal, the structure of the metal's surface, and the nature of the medium in contact with the metal's surface. The plasmon's electric field extends about 100 to 200 nanometers in a direction perpendicular to the metal surface. Any change in the material within the plasmon's field causes a change in the resonant wavelength (*i.e.*, resonance wavelength shift). The practical consequence of this extended electric field is that the SPR effect can directly monitor antibody–antigen binding when the antibodies are coated on the metal surface. No tag molecule is required to detect the binding event. Further, the amount of resonant wavelength shift, SPR shift, is proportional to the amount of binding that takes place. A capture antibody is immobilized on the metal surface. The antigen (analyte) binds to the antibody, and this binding event is read by the instrument as a SPR shift. [53]

An advantage of SPR sensing is that it does not require repeated washing steps: in theory, the sensor operates without maintenance until a positive signal is detected. However, non-specific binding may eventually degrade the sensor surface. In Figure 4-3, this fouling has rendered the first open sensor (left) ineffective. A newly opened sensor (right) is capable of detecting the presence of analyte of interest when it enters the sample stream. This concept could be applied to the substrates demonstrated by Rubina et al. or Hindsen et al. to enable a long-term, multi-analyte detector. This detector might be used where long-term, automated operation is desired, such as with unmanned aerial vehicles or distributed biowarfare agent "smoke detectors."

The ability to hermetically store and controllably release another group's sensors could result in better reliability, extended lifetime, and new sensing strategies that involve closed-loop exposure of different sensor surfaces. The most appropriate markets are those that involve high-importance sensing with infrequent inspection or maintenance.

One possible business model is to partner with a sensor company with an existing line of biowarfare or toxic agent detectors. This company would also sell the product and pay a negotiated licensing fee based on sales to the holder of the controlled-exposure patents. An alternative approach is to license the use of a sensor that has been developed at an academic or corporate research lab and to develop and sell an integrated device independently. In either case, the potential customers would include the military (whose interest is in reliable portable detection), government security agencies (monitoring of events such as inaugurations and economic summits [56]), and corporations or building owners (monitoring of facilities).

4.3 *In vivo* glucose sensing

The second application of interest is *in vivo* glucose sensing and the possibility of integrating the controlled-exposure technology with an implantable sensor. There are several appealing aspects to this application. First, the mechanism can be integrated in its current form with little additional development, as it is already designed for *in vivo* use. Second, the mechanism allows a significant improvement in the state of the art: sensor lifetime is limited by degradation, and the storage and periodic exposure of sensors could address this problem. Third, the market is large. Tens of millions of Americans have diabetes, and approximately one million more are diagnosed each year. A percentage of these patients require frequent glucose sensing to guide insulin delivery, and the market for glucose sensing is in the billions of dollars [57].

Overview of diabetes and glucose sensing

What advances would the technology enable in the marketplace? To answer this question, it is necessary to outline the diabetes problem and describe current glucose sensor technology.

Diabetes is a metabolic disorder, an inability to maintain a normal blood glucose level [58]. Patients with diabetes have a problem producing insulin, a hormone

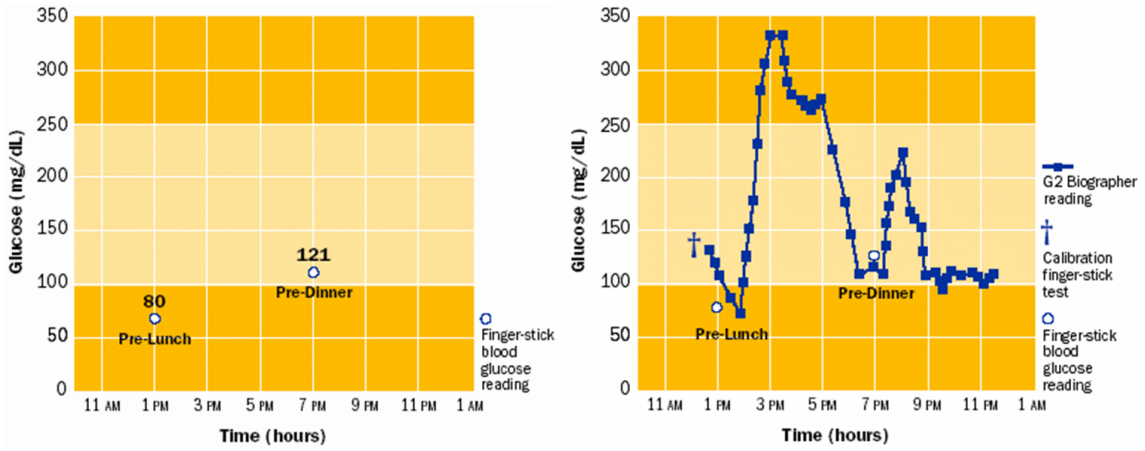

(a) (b)

Figure 4-4: Comparison of (a) occasional and (b) continuous glucose measurement [59].

normally secreted by the pancreas. Insulin mediates the transfer of glucose from the bloodstream to cells, and a deficiency of insulin causes an increase in blood glucose levels (hyperglycemia) that is physiologically harmful. The problem is managed by monitoring blood glucose levels and self-administering insulin when needed.

Blood glucose is most commonly checked by finger sticking—puncturing the skin to produce a small amount of blood and applying it to a diagnostic strip. A normal glucose level is approximately $100\,\mathrm{mg\,dL^{-1}}$; higher levels are handled by injecting insulin through a syringe or pump. However, occasional finger stick checks can miss excursions outside normal glucose levels, as illustrated in Figure 4-4. A ten-year clinical study of 1,441 volunteers showed that "keeping blood glucose levels as close to normal as possible slows the onset and progression of eye, kidney, and nerve diseases caused by diabetes" [58]. Blood glucose testing four or more times a day was an essential part of the recommended management protocol.

The health advantages identified by this study and others have prompted research into continuous sensing. Aside from a cure, the best way of managing diabetes would be what has been termed an "artificial pancreas"—a closed-loop system that would monitor blood glucose and deliver insulin whenever needed by a fully implantable or transcutaneous insulin pump. However, development of such a system has been difficult, in part due to the limitations of implantable glucose sensors.

The application analysis that follows focuses on one particular sensing mechanism: amperometric enzyme-based sensing, the most common approach. Alternate glucose measurement methods could represent competition if they are reliable and less invasive. However, no such device has been demonstrated to the standards of enzyme sensing. An example is the Glucowatch Biographer, a wristwatch-type device that operates by reverse iontophoresis [59]. However, users report that the device "burns" during operation and frequently stops working, for example during periods of excess perspiration (one user commented, "I put the watch on my outer arm, and I swear it feels like I'm getting burned. I've been able to tolerate it, but it is very uncomfortable.")

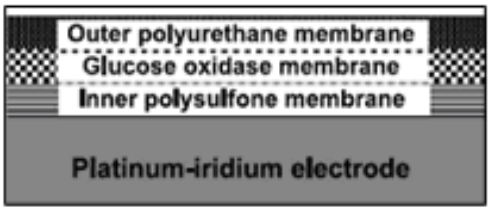

Figure 4-5: Schematic of enzyme-based amperometric glucose sensor with additional layers to block interferents and resist *in vivo* fouling [65].

[60, 61]. The company has acknowledged that skin irritation is a problem and now plans to switch to a microneedle array [62]. Other glucose measurement approaches include infrared spectroscopy, thermal radiation, ultrasonic skin poration, glucose-sensitive contact lenses, and tattooable fluorescent beads [62–64]. However, none of these devices has proved as reliable as blood or interstitial fluid testing, and these noninvasive approaches are currently limited to secondary diagnostic roles.

Amperometric enzyme-based sensing

Nearly all implantable glucose sensors rely on an enzyme-based amperometric mechanism [65]. The enzyme, glucose oxidase, catalyzes the oxidation of the glucose molecule to form hydrogen peroxide and gluconic acid. The hydrogen peroxide is then oxidized by an electrode at approximately +0.7 V (vs. Ag/AgCl) to form oxygen and water. The oxidization process at the electrode produces a current that, in theory, corresponds to the blood glucose concentration. This sensor can be used subcutaneously, as the concentration of glucose in interstitial fluid tracks with the concentration in blood with a time delay of several minutes.

A limitation to this design is that the voltage used to oxidize hydrogen peroxide also oxidizes other molecules. For example, acetaminophen and ascorbate (vitamin C) are also electroactive at 0.7 V [66]. A semipermeable membrane is therefore added over the electrode that favors the diffusion of the smaller hydrogen peroxide molecule. A suitable membrane material is a composite of cellulose acetate and Nafion, a sulfonated copolymer [67].

A second limitation is that the relatively low oxygen levels in physiological fluid threaten to make the enzyme-catalyzed reaction oxygen-limited instead of glucose-limited. An additional surrounding semipermeable membrane is necessary to promote oxygen diffusion over glucose diffusion [65]. This membrane adds an additional time delay but ensures that the oxidation current is proportional only to glucose concentration. An illustration of a sensor design with both inner and outer membranes is shown in Figure 4-5.

A third limitation is that the enzyme membrane is susceptible to fouling from macrophages, proteins, and protein fragments [68]. The oxygen-permeable outer membrane therefore handles an additional duty, that of protecting the enzyme from *in vivo* attack. Even with a barrier layer, however, the enzyme degrades over time

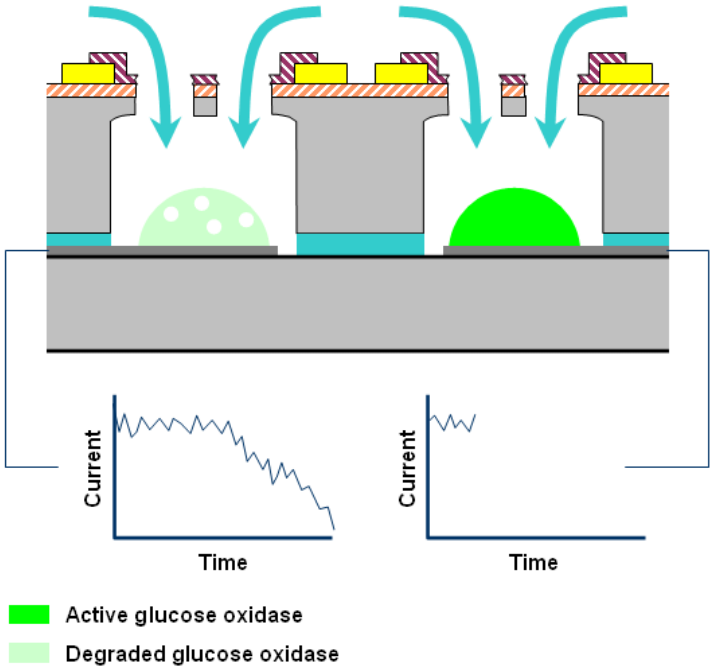

Figure 4-6: Schematic of multiple enzyme-based glucose sensors exposed by the electrothermal mechanism. The sensor exposed first (left) shows decreased amperometric current due to enzyme degradation over time. The newly exposed sensor (right) provides more reliable data.

[69]. The typical usable lifetime is several weeks, and this duration has an important effect on device use [70]. Because the sensor lifetime is too short for full surgical implantation and removal to be practical, the sensor must be inserted transcutaneously with an electrical connection to an external monitor. The FDA limits transcutaneous insertion to 72 hours because of the risk of infection. Consequently, each sensor can only be used for three days before it must be discarded.

Integration of controlled-exposure technology

The electrothermal mechanism could be integrated with this glucose sensor, and the combination of these technologies would enable a long-term device consisting of multiple short-term sensors [71]. A conceptual view is shown in Figure 4-6. After the enzyme on the first sensor (left) degrades beyond usefulness, an additional sensor (right) is exposed by microprocessor control to provide continued measurements.

The envisioned fully implantable device would contain sensors packaged in controlled-exposure cavities, a microprocessor, a telemetry antenna, and a battery, all contained within a titanium housing. With a sufficient number of hermetically sealed sensors, the implanted device could operate on the order of a year before surgical removal and replacement.

Enzymes are susceptible to degradation even if hermetically sealed, and glucose oxidase crosslinked with glutaraldehyde has a half-life of approximately ninety days

in the absence of glucose [69]. This time period is longer than if the sensor were exposed, but is still small considering the goal of implantation for at least one year. One possible solution to use an order of magnitude more enzyme than is needed for signal detection and to calibrate the device with the finger-stick method when each new sensor is exposed.

A low-melting-temperature material could be used for the membrane, as described in Chapter 3, if the material were sufficiently stable *in vivo*. This change could reduce the required voltage and therefore the required battery size—a favorable change for an implantable device.

Market value

What is the market for an implantable, continuous glucose sensor? It is helpful to identify the expected customer population and the current costs of glucose measurement. The number of expected buyers is smaller than the total diabetes population, since not all patients are frequent testers. Spurgeon et al. suggest that the expected early adopters of continuous glucose sensing devices are insulin pump users (200,000 in U.S.), patients with "brittle" or unstable diabetes (number unknown), patients unable to detect hypoglycemia (number unknown), children with diabetes (200,000), pregnant women (140,000-150,000), and technocrats (number unknown) [72].

A caveat when estimating the number of potential customers is that the fully implantable device would require a more invasive insertion procedure than the current transcutaneous needles. The needles are currently patient-inserted, while the long-term device would be implanted surgically. Still, the subcutaneous implantation procedure could be done on an outpatient basis and would only be required approximately once per year. The benefits of reduced finger stick testing (to a calibration frequency only) and continuous glucose data could convince many patients to undergo the procedure.

It is clear that a reliable continuous glucose sensor has long been desired by patients. Their anticipations and concerns are expressed in dozens of online weblogs [73]:

> Continuous monitor lust. They're starting to hit the market en force, but still aren't quite affordable or practical...And now MiniMed's new first-ever combo pump/continuous monitor system (Paradigm REAL-Time) looks pretty darn exciting, but still runs high ($1,000 on top of pump price, plus ?? [sic] sensor costs), and is still not covered by insurance. In short, waiting IMPATIENTLY for new technology to come to my aid here. Old story, new (im)patient. [74]

> OK here's the bad news [on augmenting an insulin pump with a 3-day continuous glucose sensor]: The total cost of the upgrade is $1100.00. Yeah, ouch...I have it on good authority that insurance companies (mine included, and I checked months ago) are covering the cost of the sensor purchase. Sweet. They are not, however, covering the cost of the Transmitter itself, even with a new

> pump purchase. Sour…I've got some serious raging hormones on for this sucker. No more human pincushion. No more testing twelve times a day, sometimes 15. Sometimes 20. And still managing to miss trends, knowing there's something there that I'm sure I'm JUST NOT GETTING. No more waking up five times during the damn night once a month just to make sure I'm not missing something, like a Hypo. Quicker reaction time. BG results Every Five Minutes. [75]

> [From an early user of the Medtronic Guardian 3-day continuous glucose monitor] Today I didn't have to worry about my blood sugar. The Guardian is worrying about it for me. If it goes too high she'll tell me. If it goes too low she'll tell me. So today I could focus my mind on my work, not on my diabetes. What a gift!…So do I like it? Absolutely. Is it worth what it has cost me? Double absolutely. Would I do it again? Triple absolutely. [76]

Particularly evident in the comments above is the potential buyers' concern about cost.[2] Both patients and device companies have a strong interest in insurance company reimbursement. Reimbursement is judged to be cost effective if the health advantages (quantified as "quality-adjusted life years") outweigh the management costs. The current Blue Cross policy is to reimburse expenses for cases in which frequent glucose testing is medically necessary:

> Use of invasive subcutaneous or noninvasive continuous interstitial glucose monitoring devices (*i.e.*, Minimed Continuous Glucose Monitoring System [CGMS] or the GlucoWatch Biographer) adjunct to standard care are considered medically necessary in the care of patients with Type 1 diabetes, when all of the following criteria are met:
>
> 1. Inadequate glycemic control despite compliance with frequent self-monitoring (at least four times per day) and including fasting hyperglycemia ($>150\,\mathrm{mg\,dL^{-1}}$) or … episodes of severe hypoglycemia ($<50\,\mathrm{mg\,dL^{-1}}$). This poor control is in spite of compliance with multiple alterations in self-monitoring and insulin administration regimens to optimize care; and
> 2. Insulin injections are required 3 or more times per day or an insulin pump is used for maintenance of blood sugar control; and
> 3. Four or more fingersticks are required per day. [78]

These criteria correspond to most of the patient population described above, with the exception of the technocrats (who may be willing to purchase the device out-of-pocket). As a reference, Medicare approved reimbursement of Medtronic Minimed's 3-day transcutaneous sensor four years after the FDA approved it for use and presumably after the device had been clearly demonstrated to be useful [79].

The New England Health Institute calculated that the ratio of cost to benefit for continuous glucose sensing was approximately $51,000 per quality-adjusted life year

[2]The cost of strips and meters for frequent testers is approximately $5,000 per year per patient [64, 77]. These expenses represent a majority of the total market for self-monitoring of blood glucose, estimated to be $5 billion per year [57].

[72]. Amounts less than $100,000 per quality-adjusted life year are generally thought to be favorable in the U.S. [72]. This study estimated that the continuous sensor would cost twice the amount of strips, or approximately $10,000 per year.

The use of twice the cost of strips is, in fact, a good estimate of the cost of the envisioned implant—without yet including the controlled-exposure device. Most of the components (medical device battery, titanium housing, microprocessor, and telemetry) are identical to those used in pacemakers, which cost approximately $10,000 [80, 81]. The current transcutaneous enzyme-based glucose sensors, packaged independently, cost $35 each, a small fraction of the total cost of the other implant components. The cost of the controlled-exposure microchip is proprietary to MicroCHIPS, but the information above allows an estimate on the order of $10,000 for the maximum feasible cost: if the cost of integrating the microchip is smaller than this approximate amount, then the market is favorable. The total implant price would be estimated to be $10,000–$20,000, implying a revenue on the order of $1 billion for every round of implants purchased by a patient population of 100,000. If the microchip integration cost is more than this approximate amount—that is, the complete implant cost is more than $20,000 per year per patient—then the benefit-to-cost ratio is not favorable according to the New England Health Institute's study, and insurance company reimbursement is less likely.

One possible business model is to partner with a medical device company that already has an implantable glucose sensor and experience in acquiring FDA approval. The device company would manage the FDA approval process, sell the product, and pay a negotiated licensing fee based on sales to the holder of the controlled-exposure patents.

Candidates for partnership include any company developing an implantable glucose sensor. A suitable company would need to have the resources to pursue the project through pre-clinical and clinical tests, the FDA approval process, and the time to acquire customers and insurance reimbursement.

It is impossible to guarantee that a noninvasive method of measuring blood glucose will not emerge in the next few years, making an implantable device undesirable in comparison. However, the methods attempted so far have been limited by signal interference and other difficulties in obtaining accurate readings. The (albeit invasive) enzyme-based sensor has been proved *in vivo*, as has the electrothermal mechanism. There is therefore a clear path to assembling a reliable device that satisfies patients at a cost acceptable to health care companies.

Chapter 5

Conclusions

The goal of this thesis has been to present the engineering and commercial aspects of an electrothermal controlled-exposure technology. The identification and analysis of key material properties has enabled materials selection guidelines to be generated. Additionally, favorable commercial opportunities were identified by considering the capabilities and limitations of the technology.

An electrothermal analysis of activation was found to be useful for identifying significant mechanisms of heat loss and developing guidelines for suppressing them. The observation that heat conduction through the membrane is a dominant mechanism of heat loss, for example, motivates the reduction of the membrane's thermal conductivity and thickness. In almost every case, however, approaches for optimizing materials and geometry tend to invalidate the conditions under which they are valid. That is, if optimization is successful, than the dominant heat transfer mechanism will be suppressed and the corresponding guidelines will no longer apply. The one exception is the membrane's melting temperature: it is always advantageous in terms of the activation requirements to reduce this value. However, a reduction in melting temperature could lead to problems with pinhole formation and mechanical yielding because the homologous temperature (the ratio of operating temperature to melting temperature) of the membrane material will increase.

The use of an alloy as a membrane material could have multiple benefits: the introduction of impurities tends to increase a metal's electrical resistivity and reduce its thermal conductivity, which should increase heat generation and reduce thermal losses, respectively. Additionally, solid solutions of impurities suppress dislocation and grain boundary motion, which could favorably affect membrane strength and resistance to thermal grooving. Finally, some alloy systems contain eutectics, which would further reduce the required activation temperature of the membrane. Different alloy compositions could be tested by depositing the membrane material by cosputtering and evaluating the activation requirements, strength, hermeticity, and stability of the resulting devices.

A potential area of commercialization for the electrothermal technology is sensor exposure. The most suitable types of sensors are devices that are easily miniaturized and placed in arrays for periodic exposure. In particular, electrodes and optically interrogated surfaces are well suited for this type of packaging. Macromolecules such as

enzymes and antibodies enable selectivity and sensitivity; however, these compounds are susceptible to fouling and degradation over time. The controlled storage and exposure of these sensors would improve the state of the art in the areas of biowarfare agent detection and *in vivo* glucose sensing.

The electrothermal technology has already been shown to work *in vitro* and *in vivo*. Furthermore, the electrochemical and optical sensors discussed in this thesis have been well characterized and widely used; one of their most significant disadvantages is their limited lifetime. The remaining challenge is to integrate the controlled-exposure method with these sensors at a reasonable cost and to begin bringing devices to market.

Appendix A

Electrothermal modeling

A heat transfer model is presented in this appendix for analyzing a suspended membrane undergoing resistive heating. A comprehensive study of membrane rupture is beyond the scope of this thesis; activation combines multiple thermal and mechanical effects, and even activation in air involves intricacies such as non-uniform heat generation, a solid-to-liquid phase change, and a moving interface. When activation occurs in liquid, an additional liquid-to-vapor phase change adds to the complexity. A variety of heat transfer mechanisms can influence activation, including conduction through the membrane, conduction and convection in the surrounding environment, radiation, and boiling. An analytical solution that incorporates all of these effects does not likely exist.

The approach that follows is limited to comparing the influence of heat transfer mechanisms and identifying whether any one of them dominates. It may then be possible to model some thermal aspects of activation by examining only this dominant mechanism. Some simplifying assumptions, such as temperature independence of material properties, are made. Furthermore, estimates of heat transfer values are limited to order-of-magnitude precision. The model is applied to several membrane configurations, and the predictions are found to match experimental results closely enough to be useful in directing design efforts. The equations developed in this appendix are used in Chapter 3 to guide materials selection for the membrane and traces.

A.1 Governing heat transfer equation

The approach taken here is to construct a governing equation of heat transfer, then to remove negligible terms and to simplify the equation until it can be solved analytically. Consider a square suspended membrane with thickness h, thermal conductivity k, specific heat c, density p, and electrical resistivity ρ. We assume that the temperature variation across the membrane thickness is negligible because the membrane length and width are at least two orders of magnitude larger than the thickness. The governing equation can be written by performing an energy balance at an arbitrary point on the membrane, as shown in Figure A-1, and dividing by the element volume $h \cdot dx \cdot dy$:

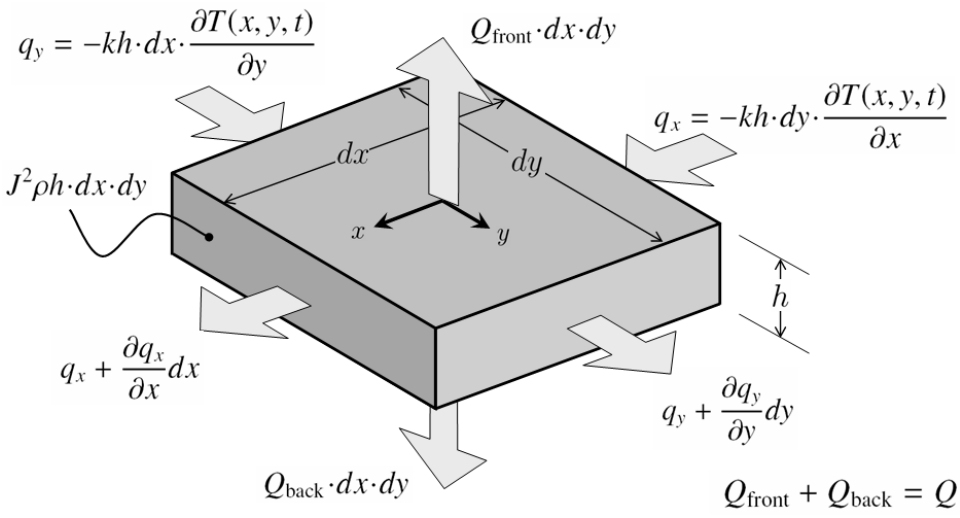

Figure A-1: Energy balance for a differential element in a suspended membrane.

$$\nabla \cdot [k \nabla T(x,y,t)] - \frac{Q}{h} + J^2 \rho = cp \frac{\partial T(x,y,t)}{\partial t} \tag{A.1}$$

In this equation, T is the temperature, $Q = Q_{\text{front}} + Q_{\text{back}}$ is the total heat flux to the surrounding medium from the top and bottom faces of the membrane, and J is the current density. The first term, which contains the Laplacian of the temperature distribution, is related to heat conduction through the membrane; the second, heat loss from the membrane faces; the third, heat generation; and the fourth, heat storage. Note that, in the most general case, the material properties are dependent on temperature, the current density is not uniform within the membrane, and the heat flux losses are different on the front and back sides of the membrane.

This equation can be simplified by assuming temperature-independent material properties and by approximating the spatial differential term with a finite difference term. The simplified equation is

$$k \frac{-\Delta T(t)}{r_0^2} - \frac{Q}{h} + J^2 \rho = cp \frac{d\Delta T(t)}{dt} \tag{A.2}$$

where ΔT is the temperature difference between the center and the edge of the membrane and r_0 is a characteristic dimension, taken to be half the side length for a square membrane.[1] The minus sign appears in the first term because we are subtracting a temperature at positive x, y from a temperature at the center of the membrane ($x = y = 0$).

[1] Other characteristic dimensions might also be used: half the diagonal of the membrane, for example, or the radius of a circle with equivalent area. A case could be made for using $r_0 = 35\,\mu\text{m}$, half the total width of the membrane (including the overlap over the substrate). As shown in Figure 2-7, the substrate overlap areas of gold membranes melt during activation, so these regions are certainly affected by membrane heating. In any case, the differences are negligible for this order-of-magnitude analysis.

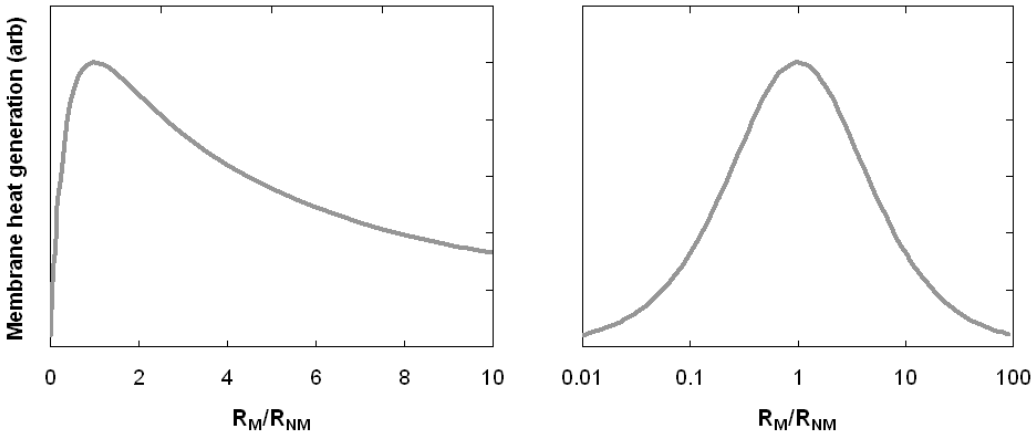

Figure A-2: Efficiency as a function of the ratio between membrane and non-membrane resistances, plotted on linear and logarithmic scales.

Maximizing heat generation

It is advantageous to maximize the volumetric heat generation Q_{gen} in the membrane for a given activation voltage. This heat generation is measured in $\mathrm{W\,m^{-3}}$ and for resistive heating is equivalent to $J^2\rho$. This term can be expanded as follows:

$$Q_{\text{gen}} = J^2\rho = \left(\frac{V}{whR}\right)^2 \rho = \frac{V^2\rho}{w^2h^2(R_{\text{M}}+R_{\text{NM}})^2} = \frac{V^2\rho}{w^2(\rho+hR_{\text{NM}})^2} \tag{A.3}$$

where w is the width of the membrane feature including the substrate overlap. The other parameters (voltage V, total circuit resistance R, membrane resistance R_{M}, and non-membrane resistance R_{NM}) remain as defined in Chapter 2. It is assumed that the membrane feature is square and that the resistivity is uniform to obtain $R_{\text{M}} = \rho/h$.

The relationship suggests the existence of an optimal value of resistivity, since current is inversely related to membrane resistance. For small values of ρ approaching zero, the heat generation in the membrane approaches zero. Alternatively, for very large values of ρ, the current becomes negligible, and the heat generation term again approaches zero. The arrangement that maximizes volumetric heat generation (acquired by setting $\frac{\partial Q_{\text{gen}}}{\partial \rho}$ equal to zero) occurs at $\rho = hR_{\text{NM}}$, where the membrane resistance equals the non-membrane resistance. This point corresponds to the optimal power matching between the power source (the battery or capacitor) and the intended power sink (the membrane). The relationship between the resistances and the heat generation efficiency is shown in Figure A-2, in which the ratio is plotted on both linear and logarithmic scales.

A.2 Identifying a dominant heat transfer mode

A single heat transfer mechanism (conduction through the membrane, conduction to the surrounding medium, radiation, or boiling) may have considerably more influence

Table A.1: Properties of selected membrane and surrounding medium materials (taken at 25°C except for heat of melting, which is taken at the melting temperature.)

Material	Thermal conductivity k ($\mathrm{W\,m^{-1}\,K^{-1}}$)	Specific heat c ($\mathrm{J\,kg^{-1}\,K^{-1}}$)	Density p ($\mathrm{kg\,m^{-3}}$)	Resistivity ρ ($n\Omega\,\mathrm{m}$)	Melting temp. T_m (°C)	Heat of melting H_m ($\mathrm{kJ\,kg^{-1}}$)
Gold	320	130	19100	22	1064	64
Titanium	20	520	4500	420	1668	296
Water	0.6	4200	1000			
Air	0.03	1000	1.2			

than the others, which can then be neglected. As a practical example, MicroCHIPS has prototyped square 50 μm × 50 μm gold membranes with a thickness of 0.6 μm and electrothermally ruptured these membranes in air and water. This configuration serves as a good model for comparing the different mechanisms of heat transfer related to air and water immersion and evaluating the case of one dominant mechanism (in this case, membrane conduction).

Conduction through the membrane

It is assumed that a sufficient current is applied to heat at least a portion of the gold membrane to the melting temperature. An order-of-magnitude estimate of the first term in Equation (A.2) can be acquired by using the material properties of bulk gold at room temperature (Table A.1) and by taking ΔT to be the difference between the melting temperature and room temperature. With $r_0 = 25\,\mu\mathrm{m}$, the membrane conduction term $k\Delta T/r_0^2$ is estimated to be between 10^{14} and $10^{15}\ \mathrm{W\,m^{-3}}$.

Conduction to the surrounding medium

The surrounding medium is taken to be air (the value of Q/h in the case of water immersion is addressed below). Heat conduction to the surrounding medium can be estimated by assuming a semi-infinite medium on both sides of the membrane. The heat flux from each side at time t is [82]

$$\Delta T\sqrt{\frac{k_\mathrm{m}c_\mathrm{m}p_\mathrm{m}}{\pi t}} \tag{A.4}$$

where k_m, c_m, and p_m are the thermal conductivity, specific heat, and density of the surrounding medium, respectively. The average value Q_med/h from both sides during the activation time t_act is therefore

$$\frac{Q_\mathrm{med}}{h} = \frac{2}{t_\mathrm{act}h}\int_0^{t_\mathrm{act}} \Delta T\sqrt{\frac{k_\mathrm{m}c_\mathrm{m}p_\mathrm{m}}{\pi t}}dt = \frac{4\Delta T}{h}\sqrt{\frac{k_\mathrm{m}c_\mathrm{m}p_\mathrm{m}}{\pi t_\mathrm{act}}} \tag{A.5}$$

Material properties of air are given in Table A.1. Assuming an activation pulse length of 10 to 100 μs (as is typically observed in experiments), this term is estimated to be between 10^{12} and $10^{13}\,\mathrm{W\,m^{-3}}$, roughly two orders of magnitude less than conduction through the membrane.

Radiation exchange with the surrounding medium

The magnitude of radiation transfer from both sides of the membrane is estimated by [82]

$$\frac{Q_{\mathrm{rad}}}{h} = \frac{2\sigma}{h}\left(T^4 - T_\infty^4\right) \tag{A.6}$$

where σ is the Stefan-Boltzmann constant ($5.67\times10^{-8}\,\mathrm{W\,m^{-2}\,K^{-4}}$) and T_∞ is the ambient temperature. The surface emissivity is assumed to be unity on both sides of the membrane. The maximum radiation transfer value, assuming a uniform membrane temperature of 1064°C, is estimated to be between 10^{11} and $10^{12}\,\mathrm{W\,m^{-3}}$. This is roughly three orders of magnitude less than the membrane conduction value.

Boiling heat transfer

The surrounding medium is now taken to be water. Vapor bubbles observed by high-speed photography indicate that boiling does occur as the membrane electrothermally heats and ruptures in water. The magnitude of heat flux to assign to this mechanism is uncertain, however. Literature indicate that for a temperature difference of 1000°C, the steady-state boiling heat flux, which includes conduction and radiation effects, can be as high as approximately $10^{6}\,\mathrm{W\,m^{-2}}$ from each side of the membrane (Figure A-3). This corresponds to a Q/h value between 10^{12} and $10^{13}\,\mathrm{W\,m^{-3}}$. However, higher instantaneous values of boiling heat flux (some as large as hundreds of $\mathrm{W\,m^{-2}}$) have also been reported for suspended platinum wires [32, 83] and microscale resistive heaters [84, 85]. The theoretical upper limit of heat flux in a vaporization process has been predicted to be $223\,\mathrm{W\,m^{-2}}$ [86, 87], which would result in a Q/h value of larger than $10^{14}\,\mathrm{W\,m^{-3}}$. The range of possible estimates for boiling heat transfer is therefore several orders of magnitude, with the maximum value in the same order of magnitude as that of membrane conduction.

Membrane heat conduction as a dominant mode

It is estimated from the calculations above that conduction through the membrane is the primary mode of heat loss for this particular configuration except when considering the highest available estimates of boiling heat flux. For conduction-dominated operation, the temperature distribution in the membrane is expected to be a strong function of the distance to the edge of the substrate. It is also expected that the melted area would originate at the center of the membrane and grow larger with increased current. This effect has indeed been observed in gold membranes tested in air and water.

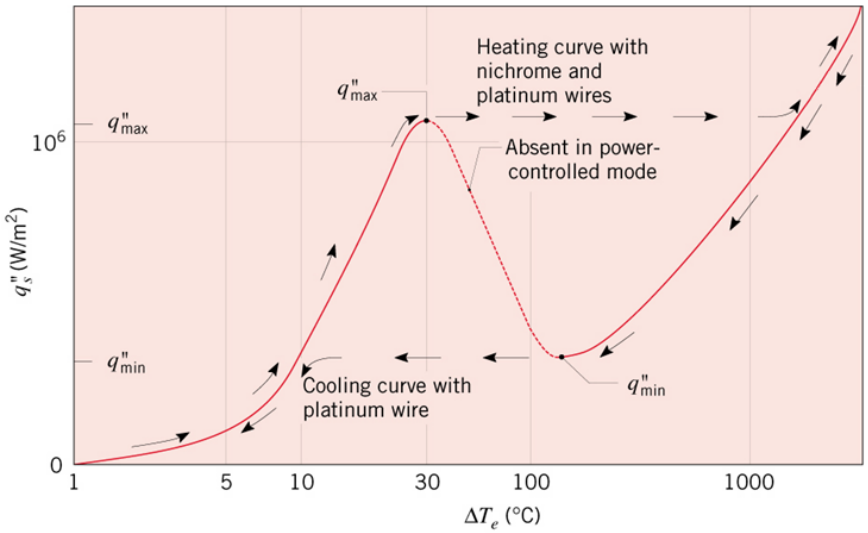

Figure A-3: Boiling heat flux and regimes in water as a function of excess temperature [82].

The simplified version of Equation (A.2), considering only membrane heat conduction, is

$$-k\frac{\Delta T(t)}{r_0^2} + J^2\rho = cp\frac{d\Delta T(t)}{dt} \tag{A.7}$$

whose solution provides the time-dependent temperature at the center of the membrane:

$$\Delta T(t) = \frac{J^2\rho r_o^2}{k}\left[1 - \exp(-tk/cpr_0^2)\right] \tag{A.8}$$

The minimum required current and voltage to heat the center of the membrane to its melting temperature are calculated from Equation (A.8) to be:

$$I_{\text{req}} = 2r_0hJ = 2h\sqrt{\frac{k\Delta T}{\rho}} \tag{A.9}$$

$$V_{\text{req}} = I_{\text{req}}R = 2h(R_{\text{M}} + R_{\text{NM}})\sqrt{\frac{k\Delta T}{\rho}} = 2(\rho + hR_{\text{NM}})\sqrt{\frac{k\Delta T}{\rho}} \tag{A.10}$$

The minimum required current for a 0.6 µm-thick, 50 µm × 50 µm gold membrane is estimated from Equation (A.9) to be 4 A. The actual minimum current was found to be 5.7 A in both air and water, confirming that boiling and conduction to the surrounding medium have a negligible influence on operation for this particular configuration. The predicted and measured minimum current values are in good agreement considering the simplifications that were made (temperature-independent material properties, differentials approximated by finite differences, and an approximated characteristic dimension of half the membrane side length).

The characteristic size r_0 does not appear in the current estimate in Equation (A.9), suggesting that membrane size does not have a strong effect on the required current. This prediction has also been confirmed in experiments: a 0.6 μm-thick, 100 μm × 100 μm membrane required 6 A to open in air and 7.3 A in water. This is a relatively small current increase considering that the membrane area has increased fourfold. Note that the activation currents are different in air and water for this configuration. As the membrane size is increased, the membrane conduction term (which scales with r_0^{-2}) correspondingly decreases until this term no longer dominates.

Finally, a similar dependence on membrane resistivity is seen in Equation (A.10) that was seen in Equation (A.3). Either a very small or very large resistivity value leads to a large current and voltage requirement, and an optimal point must lie somewhere in between. An additional subtlety is that for metals the thermal conductivity k is coupled (inversely) to resistivity ρ and will also vary with materials substitution.

Membrane heat conduction as a non-dominant mode

The relationships derived above assume that heat loss is dominated by conduction through the membrane. Configurations in which this is not the case are subject to other governing equations, and these equations are more difficult to derive due to nonlinear relationships between temperature and heat flow, particularly in the case of radiation and boiling. We can at least note that the other methods of heat loss—conduction to the surrounding medium, radiation, and boiling—all involve heat flux normal to the membrane. If one of these mechanisms were to dominate, we would expect little temperature variation across the membrane and melting to occur more or less uniformly at a threshold current level.

It would be interesting to examine the behavior of a membrane for which boiling is the dominant method of heat loss. The most prominent experimental feature would be a required current for operation in liquid that is far higher than the required current for operation in air. However, MicroCHIPS has not yet prototyped such a membrane configuration. The closest example may be Pt/Ti/Pt membranes with a titanium thickness of 0.3 μm.[2] Activation tests of this configuration resulted in noticeably different current requirements when the membranes were immersed fully or partially in water or immersed in air. The current-activation time relationships for this configuration are shown in Figure A-4. The different results for different surrounding media indicate that membrane conduction no longer dominates over all of the other terms in Equation (A.2), as it did for the 0.6 μm-thick gold configuration considered earlier. The change is likely due to the change in material (the thermal conductivity of titanium is less than one tenth of the thermal conductivity of gold, as shown in Table A.1), and the reduction of the membrane thickness.

[2] These membranes were coated with a 10 to 20 nm platinum layer on both sides to suppress titanium oxidation.

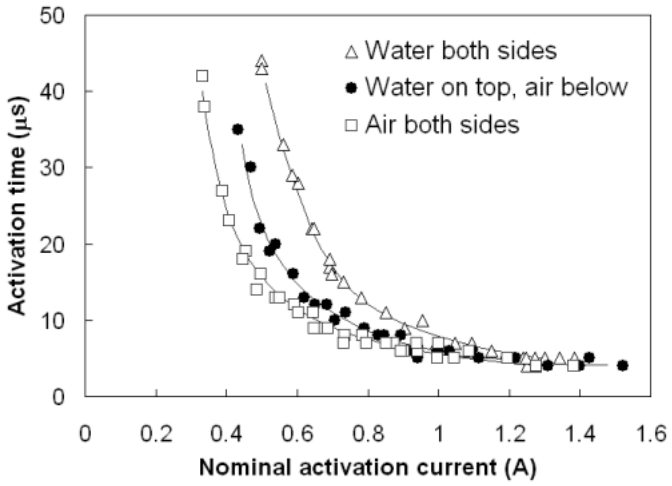

Figure A-4: Opening area as a function of activation current for a 0.34 μm-thick, 50 μm × 50 μm Pt/Ti/Pt membrane immersed in air, air/water, and water [11].

Activation energy, time, and thermal impact

Let us again consider membrane configurations in which membrane conduction is the dominant heat transfer mode. From Equation (A.8), the activation time t_{act} and energy dissipated near the membrane E_{M} are estimated to scale as

$$t_{\text{act}} \propto \ln\left(1 - \frac{I_{\text{req}}^2}{I^2}\right) \tag{A.11}$$

$$E_{\text{M}} = I^2 R_{\text{M}} t_{\text{act}} \propto I^2 R_{\text{M}} \ln\left(1 - \frac{I_{\text{req}}^2}{I^2}\right) \tag{A.12}$$

These relationships are shown graphically in Figure A-5(a), where the excess activation current is defined to be the ratio of I to I_{req}. At $I < I_{\text{req}}$, the current is too low to rupture the membrane in any reasonable time, and activation does not occur. At $I > I_{\text{req}}$, activation occurs in a finite time and dissipates some finite amount of energy. The time and energy values both decrease with increasing current; the time approaches zero, while the energy approaches the minimum amount needed to heat the membrane alone to its melting temperature and to melt it. This minimum energy can be written as

$$E_{\text{M,min}} = 4r_0^2 h \int_{T_\infty}^{T_{\text{m}}} cp\, dT + 4r_0^2 hpH_{\text{m}} \approx 4r_0^2 hp(c\Delta T + H_{\text{m}}) \tag{A.13}$$

where T_{m} is the melting temperature, H_{m} is the heat of melting for the membrane material, and the last (approximate) term assumes temperature-independent specific heat and density. This value is the lower bound for the energy required for the electrothermal mechanism. We can estimate this lower bound using the properties given in Table A.1, assuming constant specific heat and density. For 0.3 μm-thick,

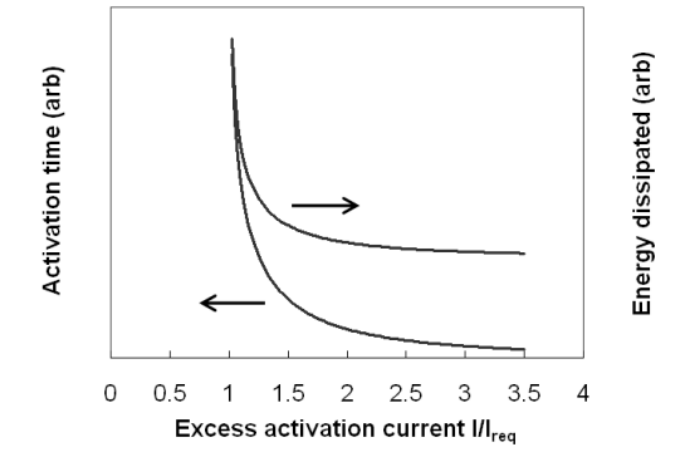

(a)

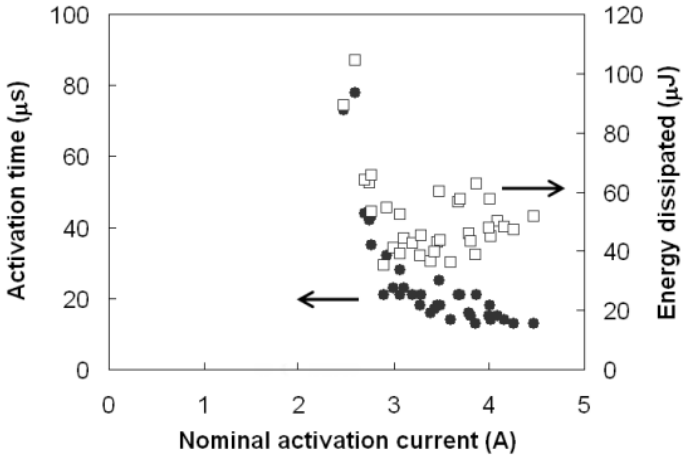

(b)

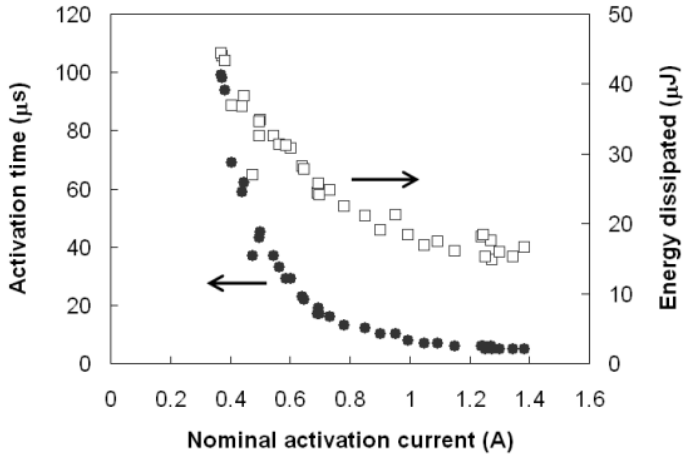

(c)

Figure A-5: Activation time and energy dissipated near the membrane for (a) theoretical case and (b,c) experimental results of 50 µm × 50 µm gold and Pt/Ti/Pt membranes, respectively, activated in water [11].

50 μm × 50 μm membranes, the energy is 1.8 + 0.9 = 2.7 μJ for gold and 2.9 + 1.0 = 3.9 μJ for titanium. The first number in each case represents the energy need to heat the membrane to its melting point, and the second represents the energy required for melting.

Experimental measurements of activation time and dissipated membrane energy as a function of current are shown in Figure A-5(b) and (c) for 0.3 μm-thick, 50 μm × 50 μm gold and Pt/Ti/Pt membranes, respectively. The activation times were measured by observing the current traces as shown in Figure 2-6. This energy is calculated by integrating the power generation within the membrane:

$$E_{\mathrm{M}} = \int I^2 R_{\mathrm{M}}\, dt = \int (VI - I^2 R_{\mathrm{NM}})\, dt \approx \sum \left[\Delta t (VI - I^2 R_{\mathrm{NM}})\right] \tag{A.14}$$

The membrane resistance R_{M} varies with temperature and is not specifically measured over time. However, the integrand can be rewritten as the difference between the total energy and the energy dissipated in the traces and electronics [1]. The non-membrane resistance R_{NM}, which includes the traces and electronics, is constant and known, and the current I is measured over time as shown in Figure 2-6. The integral is approximated by summing the data points in Figure 2-6, where the sampling interval Δt is 1 μs.

The results are at least qualitatively similar; at large current values, activation takes between 10 and 20 μs for gold membranes and just a few microseconds for Pt/Ti/Pt membranes. Below a certain current value, activation does not occur within over one hundred microseconds.

Two important points should be noted. First, the activation time in practice does not asymptotically approach zero but rather the time for the membrane to physically rupture. It appears from Figures A-5(b) and (c) that this rupture time is not greater than approximately 15 μs for gold membranes or 5 μs for Pt/Ti/Pt membranes. Second, the actual energy is always greater than the theoretical minimum energy, for several reasons. The temperature distribution is not perfectly uniform, as is assumed in Equation (A.13). Additionally, some energy is dissipated at the areas of substrate overlap and during the rupture period; these additional factors are not considered in Equation (A.13). Finally, the minimum energy point can only be approached asymptotically at large currents and short time scales.

It is useful when evaluating thermal effects to consider the energy E_{M} dissipated in the membrane area during activation. The energy dissipated near the membrane is roughly 40 to 60 μJ for both gold and Pt/Ti/Pt membranes. This value is barely enough to heat one microgram (one nanoliter) of water by a temperature increase of 10°C. Assuming that the cavity contents can be modeled with the properties of liquid water, this temperature increase coupled to this amount of material—both values being upper bounds—is negligible for all applications considered so far.

A.3 Summary of electrothermal model

The analysis described above leads to the following conclusions:

- Heat generation is maximized at a given voltage by minimizing the non-membrane resistance and by designing a membrane with resistance equal to the remaining non-membrane resistance. This approach provides the optimal power transfer from the energy source to the membrane.

- The heat transfer analysis is simplified by comparing the magnitude of heat transfer mechanisms, even to order-of-magnitude resolution, and by ignoring the smaller terms. Membrane activation experiments support the validity of this simplification in the case where conduction through the membrane is the dominant mechanism of heat loss.

- In cases in which heat conduction through the membrane dominates, the required voltage can be reduced by using a thinner membrane or a membrane material with a smaller thermal conductivity. These changes, however, tend to reduce the chance that heat conduction through the membrane will continue to dominate.

- A higher instantaneous current results in faster operation and reduces the amount of energy dissipated near the membrane asymptotically to a lower limit. This lower limit is always larger than the energy required to heat and melt the membrane alone with no external losses.

Bibliography

[1] J M Maloney, S A Uhland, B F Polito, N F Sheppard, C M Pelta, and J T Santini. Electrothermally activated microchips for implantable drug delivery and biosensing. *J Control Release*, 109(1-3):244–255, 2005.

[2] Kirsner, S, 2004. The right dose via microchip. *Boston Globe*, Feb 23, 2004.

[3] R Langer. Biomaterials for drug delivery and tissue engineering. *MRS Bulletin*, 31:477–485, 2006.

[4] J T Santini. *A controlled-release microchip*. PhD thesis, Massachusetts Institute of Technology, 1999.

[5] J T Santini, M J Cima, and R Langer. A controlled-release microchip. *Nature*, 397(6717):335–338, 1999.

[6] Y Li, R S Shawgo, B Tyler, P T Henderson, J S Vogel, A Rosenberg, P B Storm, R Langer, H Brem, and M J Cima. *In vivo* release from a drug delivery MEMS device. *J Control Release*, 100(2):211–219, 2004.

[7] R S Shawgo, G Voskerician, H L Duc, Y Li, A Lynn, M MacEwan, R Langer, J M Anderson, and M J Cima. Repeated *in vivo* electrochemical activation and the biological effects of microelectromechanical systems drug delivery device. *J Biomed Mater Res*, A 71(4):559–568, 2004.

[8] Y Li, H L Ho Duc, B Tyler, T Williams, M Tupper, R Langer, H Brem, and M J Cima. *In vivo* delivery of BCNU from a MEMS device to a tumor model. *J Control Release*, 106(1-2):138–145, 2005.

[9] S A Uhland, B F Polito, J M Maloney, N F Sheppard, S J Herman, and B Y Yomtov. Controlled release device and method using electrothermal ablation, US patent application 2004/0121486.

[10] A M Johnson. *Noninvasive quantification of drug delivery from an implantable MEMS device*. PhD thesis, Massachusetts Institute of Technology, 2004.

[11] Reprinted with permission of MicroCHIPS, Inc.

[12] J H Prescott, S Lipka, S Baldwin, N F Sheppard, J M Maloney, J Coppeta, B Yomtov, M A Staples, and J T Santini. Chronic, programmed polypeptide delivery from an implanted, multireservoir microchip device. *Nat Biotechnol*, 24(4):437–438, 2006.

[13] J T Santini. Microchips for implantable drug delivery and biosensing. MIT MTL VLSI Lecture Series, Mar 2006.

[14] L V V Pakalapati. *Controlled release microchip*. Master's thesis, Massachusetts Institute of Technology, 2003.

[15] J T Santini, Z Sbiaa, and J R Coppeta. Multi-cap reservoir devices for controlled release or exposure of reservoir contents, US patent application 2006/0057737.

[16] S A Uhland, B F Polito, S J Herman, J T Santini, and J M Maloney. Hermetically sealed microchip reservoir devices, US patent application 2005/0077584.

[17] M J Madou. *Fundamentals of Microfabrication: The Science of Miniaturization, Second Edition*. CRC, 2002.

[18] T Diepold and E Obermeier. Smoothing of ultrasonically drilled holes in borosilicate glass by wet chemical etching. *J Micromech Microeng*, 6(1):29–32, 1996.

[19] E Belloy, S Thurre, E Walckiers, A Sayah, and M A M Gijs. The introduction of powder blasting for sensor and microsystem applications. *Sensors Actuators*, A 84:330–337, 2000.

[20] X Li, T Abe, and M Esashi. Deep reactive ion etching of Pyrex glass using SF_6 plasma. *Sensors Actuators*, A 87:139–145, 2001.

[21] D Smigiel, K Domanski, P Prokaryn, and P Grabiec. Deep etching of biocompatible silicone rubber. *Microelec Eng*, 83(4-9):1178–1181, 2006.

[22] M C Lai and E M Topp. Solid-state chemical stability of proteins and peptides. *J Pharm Sci*, 88(5):489–500, 1999.

[23] K Fu, A M Klibanov, and R Langer. Protein stability in controlled-release systems. *Nat Biotechnol*, 18(1):24–25, 2000.

[24] H Greenhouse. *Hermeticity of Electronic Packages (Materials Science and Process Technology)*. Noyes Publications, 2000.

[25] L Massey. *Permeability Properties of Plastics and Elastomers: A Guide to Packaging and Barrier Materials*. Plastics Design Library, 2003.

[26] R H Doremus. *Diffusion of Reactive Molecules in Solids and Melts*. Wiley-Interscience, 2001.

[27] M Stavola, J R Patel, L C Kimerling, and P E Freeland. Diffusivity of oxygen in silicon at the donor formation temperature. *App Phys Lett*, 42(1):73–75, 1983.

[28] T Onishi, E Iwamura, K Takagi, and K Yoshikawa. Influence of adding transition metal elements to an aluminum target on electrical resistivity and hillock resistance in sputter-deposited aluminum alloy thin films. *J Vac Sci Tech*, 14(5):2728–2735, 1996.

[29] W F Gale and T C Totemeier. *Smithells Metals Reference Book, Eighth Edition*. Butterworth-Heinemann, 2004.

[30] J H Westbrook and R L Fleischer. *Intermetallic Compounds: Principles and Practices, Volume 1*. John Wiley and Sons, 2000.

[31] C T Avedisian, W S Osborne, F D McLeod, and C M Curley. Measuring bubble nucleation temperature on the surface of a rapidly heated thermal ink-jet heater immersed in a pool of water. *Proc Royal Soc London*, A 455:3875–3899, 1999.

[32] S Glod, D Poulikakos, Z Zhao, and G Yadigaroglu. An investigation of microscale explosive vaporization of water on an ultrathin Pt wire. *Int J Heat Mass Transfer*, 45(2):367–379, 2002.

[33] J Li, G P Peterson, and P Cheng. Mechanical nonequilibrium considerations in homogeneous bubble nucleation for unsteady-state boiling. *Int J Heat Mass Transfer*, 48:3081–3096, 2005.

[34] H Lee, R A Coutu, S Mall, and K D Leddy. Characterization of metal and metal alloy films as contact materials in MEMS switches. *J Micromech Microeng*, 16(3):557–563, 2006.

[35] H D Espinosa and B C Prorok. Size effects on the mechanical behavior of gold thin films. *J Mat Sci*, 38(20):4125–4128, 2003.

[36] R Abbaschian and R E Reed-Hill. *Physical Metallurgy Principles*. Thomson-Engineering, 1991.

[37] J D Brazzle, W P Taylor, B Ganesh, J J Price, and J J Bernstein. Solution hardened platinum alloy flexure materials for improved performance and reliability of MEMS devices. *J Micromech Microeng*, 15(1):43–48, 2005.

[38] M J Cima, J T Santini, and S J Herman. Device for controlled reservoir opening with reinforced reservoir caps, US patent application 2005/0143715.

[39] C H Tsau, S M Spearing, and M A Schmidt. Fabrication of wafer-level thermocompression bonds. *J Microelectromech Sys*, 11(6):641–647, 2002.

[40] E Jiran and C V Thompson. Capillary instabilities in thin, continuous films. *Thin Solid Films*, 208(1):23–28, 1992.

[41] Easterling E and D A Porter. *Phase Transformations in Metals and Alloys, Second Edition*. CRC, 1992.

[42] R E Hummel, R T DeHoff, S Matts-Goho, and W M Goho. Thermal grooving, thermotransport and electrotransport in doped and undoped thin gold-films. *Thin Solid Films*, 78(1):1–14, 1981.

[43] C V Thompson. Grain growth in thin films and strips. 1st International Conference on Recrystallization and Grain Growth, Aachen, Germany, Aug 2001.

[44] Center for Counterproliferation Research, National Defense University, 2003. *Toward a national biodefense strategy: challenges and opportunities*. Accessed online at http://www.ndu.edu/centercounter/CCR%202003.pdf on July 25, 2006.

[45] Centers for Disease Control and Prevention, 2006. Accessed online at http://www.cdc.gov on May 14, 2006.

[46] Committee on Materials and Manufacturing Processes for Advanced Sensors, National Research Council of the National Academies, 2004. *Sensor systems for biological agent attacks: protecting buildings and military bases*. National Academies Press.

[47] B M Paddle. Biosensors for chemical and biological agents of defence interest. *Biosens Bioelectron*, 11(11):1079–1113, 1996.

[48] S S Iqbal, M W Mayo, J G Bruno, B V Bronk, C A Batt, and J P Chambers. A review of molecular recognition technologies for detection of biological threat agents. *Biosens Bioelectron*, 15:549–578, 2000.

[49] D V Lim, J M Simpson, E A Kearns, and M F Kramer. Current and developing technologies for monitoring agents of bioterrorism and biowarfare. *Clin Microbiol Rev*, 18(4):583–607, 2005.

[50] J J Gooding. Biosensor technology for detecting biological warfare agents: recent progress and future trends. *Anal Chim Acta*, 559:137–151, 2006.

[51] M T McBride, S Gammon, M Pitesky, T W OŠBrien, T Smith, J Aldrich, R G Langlois, B Colston, and K S Venkateswaran. Multiplexed liquid arrays for simultaneous detection of simulants of biological warfare agents. *Anal Chem*, 75:1924–1930, 2003.

[52] B J Hindson, M T McBride, A J Makarewicz, B D Henderer, U S Setlur, S M Smith, D M Gutierrez, T R Metz, S L Nasarabadi, K S Venkateswaran, S W Farrow, B W Colston Jr., and J M Dzenitis. Autonomous detection of aerosolized biological agents by multiplexed immunoassay with polymerase chain reaction confirmation. *Anal Chem*, 77:284–289, 2005.

[53] TRW Systems and Information Technology Group, 2001. *Biological detection system technologies technology and industrial base study*. Accessed online at http://www.acq.osd.mil/ott/natibo/docs/BioDetectReport-2.pdf on July 25, 2006.

[54] A N Naimushin, C B Spinelli, S D Soelberg, T Mann, R C Stevens, T Chinowsky, P Kauffman, S Yee, and C E Furlong. Airborne analyte detection with an aircraft-adapted surface plasmon resonance sensor system. *Sensors Actuators*, B 104(2):237–248, 2005.

[55] A Y Rubina, V I Dyukova, E I Dementieva, A A Stomakhin, V A Nesmeyanov, E V Grishin, and A S Zasedatelev. Quantitative immunoassay of biotoxins on hydrogel-based protein microchips. *Anal Biochem*, 340(2):317–329, 2005.

[56] L E Lindler, F J Lebeda, and G W Korch. *Biological Weapons Defense: Infectious Diseases and Counterbioterrorism (Infectious Disease)*. Humana Press, 2005.

[57] J Sandred, 2004. $1 billion medical deal: Abbott Labs to buy Therasense, maker of glucose monitors. *San Francisco Chronicle*, Jan 1, 2004. Accessed online at http://www.sfgate.com/cgi-bin/article.cgi?file=/chronicle/archive/2004/01/14/BUGSC49CO01.DTL&type=business on May 15, 2006.

[58] NDIC, 2006. Diabetes control and complications trial. Accessed online at http://diabetes.niddk.nih.gov/dm/pubs/control/index.htm on May 15, 2006.

[59] Glucowatch, 2006. Accessed online at http://glucowatch.com on May 17, 2006.

[60] Weaver, K, 2004. Accessed online at http://www.kweaver.org/archives/gadgets/glucowatch/index.html on May 15, 2006.

[61] J Gillis. New devices may free diabetes from constant monitoring. *Washington Post*, Apr 2006. Accessed online at http://www.washingtonpost.com/wp-dyn/content/article/2006/04/22/AR2006042201354.html on May 17, 2006.

[62] Davis, J L, 2006. Glucose meters: what's on the horizon? Accessed online at http://www.webmd.com/content/Article/107/108638.htm?pagenumber=1 on May 15, 2006.

[63] J Pickup, O Rolinski, and D Birch. *In vivo* glucose sensing for diabetes management: progress towards non-invasive monitoring. *British Med Journal*, 319(7220):1289–1289, 1999.

[64] Mendosa, D, 2006. On-line diabetes resources. Accessed online at http://www.diabetesmonitor.com/meters.htm on May 15, 2006.

[65] W K Ward, L B Jansen, E Anderson, G Reach, J C Klein, and G S Wilson. A new amperometric glucose microsensor: *in vitro* and short-term *in vivo* evaluation. *Biosens Bioelectron*, 17(3):181–189, 2002.

[66] G Palleschi, M A Rahni, G J Lubrano, J N Ngwainbi, and G G Guilbault. A study of interferences in glucose measurements in blood by hydrogen peroxide based glucose probes. *Anal Biochem*, 159(1):114–121, 1986.

[67] Y Zhang, Y Hu, G S Wilson, D Moatti-Sirat, V Poitout, and G Reach. Elimination of the acetaminophen interference in an implantable glucose sensor. *Anal Chem*, 66(7):1183–1188, 1994.

[68] N Wisniewski, B Klitzman, B Miller, and W M Reichert. Decreased analyte transport through implanted membranes: differentiation of biofouling from tissue effects. *J Biomed Mater Res*, 57(4):513–521, 2001.

[69] T I Valdes and F Moussy. *In vitro* and *in vivo* degradation of glucose oxidase enzyme used for an implantable glucose biosensor. *Diabetes Technol Ther*, 2(3):367–376, 2000.

[70] A Heller. Implanted electrochemical glucose sensors for the management of diabetes. *Annu Rev Biomed Eng*, 1:153–175, 1999.

[71] J T Santini, N F Sheppard, C C Young, and R S Langer. Microfabricated devices for the storage and selective exposure of chemicals and devices, US patent 6,849,463.

[72] S A Spurgeon, 2005. *Continuous glucose monitoring: innovation in the management of diabetes*. New England Healthcare Institute Innovation Series. Accessed online at www.nehi.net/CMS/admin/cms/_uploads/docs on August 1, 2006.

[73] DiabetesMonitor, 2006. Accessed online at http://www.diabetesmonitor.com/blogs.htm on May 14, 2006.

[74] DiabetesMine, 2006. Accessed online at http://www.diabetesmine.com/2006/04/are_we_done_yet.html on May 16, 2006.

[75] CandidDiabetes, 2006. Accessed online at http://www.candiddiabetes.com/candid_diabetes/2006/04/index.html on May 16, 2006.

[76] Dubois, W, 2005. Accessed online at http://lifeafterdx.blogspot.com on May 17, 2006.

[77] Canadian Diabetes Association, 2003. Diabetes: an investment for the future health of Canadians. Accessed online at http://www.diabetes.ca/files/Standing%20Committee%20on%20finance.doc on May 15, 2006.

[78] Blue Cross, 2006. Medical policy for glucose monitoring and related supplies. Accessed online at http://medpolicy.bluecrossca.com/policies/DME/glucose_monitoring.html on May 15, 2006.

[79] Minimed, 2006. Company history. Accessed online at http://www.minimed.com/about/history.html on May 17, 2006.

[80] A Tsao, 2003. Medtronic and St. Jude: pumping profits. *Business Week*, Mar 23, 2003. Accessed online at http://www.businessweek.com/bw50/content/mar2003/a3826093.htm on May 14, 2006.

[81] Robotham, J, 2004. Patients march to beat of different pacemaker. *Sydney Morning Herald*, May 20, 2004. Accessed online at http://www.smh.com.au/articles/2004/05/20/1085028467075.html?from=storylhs on May 17, 2006.

[82] F P Incropera and D P DeWitt. *Fundamentals of Heat and Mass Transfer, Fifth Edition*. Wiley, 2001.

[83] S A Zhukov, S Y Afanas'ev, and S B Echmaev. Concerning the magnitude of the maximum heat flux and the mechanisms of superintensive bubble boiling. *Int J Heat Mass Transfer*, 46:3411–3427, 2003.

[84] Y Hong, N Ashgriz, and J Andrews. Experimental study of bubble dynamics on a micro heater induced by pulse heating. *J Heat Transfer*, 126(2):259–271, 2004.

[85] P Deng, Y-K Lee, and P Cheng. An experimental study of heater size effect on micro bubble generation. *Int J Heat Mass Transfer*, 49:2535–2544, 2006.

[86] R W Schrage. *A Theoretical Study of Interphase Mass Transfer*. Columbia University Press, 1953.

[87] Z Zhao, S Glod, and D Poulikakos. Pressure and power generation during explosive vaporization on a thin-film microheater. *Int J Heat Mass Transfer*, 43:281–296, 2000.